Genetic and chemical control of tuberculostearic acid production in Mycobacterium avium subspecies paratuberculosis

John P Bannantine, Shannon C Duffy, María A Colombatti Olivieri, Marcel A Behr, Franck Biet, Neil P J Price

Genetic and chemical control of tuberculostearic acid production in *Mycobacterium avium* subspecies *paratuberculosis*

John P. Bannantine,[1] Shannon C. Duffy,[2] María A. Colombatti Olivieri,[1,3] Marcel A. Behr,[2] Franck Biet,[4] Neil P. J. Price[5]

AUTHOR AFFILIATIONS See affiliation list on p. 20.

ABSTRACT Tuberculostearic acid (TBSA) is a fatty acid unique to mycobacteria and some corynebacteria and has been studied due to its diagnostic value, biofuel properties, and role in membrane dynamics. In this study, we demonstrate that TBSA production can be abrogated either by addition of pivalic acid to mycobacterial growth cultures or by a *bfaA* gene knockout encoding a flavin adenine dinucleotide (FAD)-binding oxidoreductase. *Mycobacterium avium* subspecies *paratuberculosis* (*Map*) growth and TBSA production were inhibited in 0.5-mg/mL pivalic acid-supplemented cultures, but higher concentrations were needed to have a similar effect in other mycobacteria, including *Mycobacterium smegmatis*. While *Map* C-type strains, isolated from cattle and other ruminants, will produce TBSA in the absence of pivalic acid, the S-type *Map* strains, typically isolated from sheep, do not produce TBSA in any condition. A SAM-dependent methyltransferase encoded by *bfaB* and FAD-binding oxidoreductase are both required in the two-step biosynthesis of TBSA. However, S-type strains contain a single-nucleotide polymorphism in the *bfaA* gene, rendering the oxidoreductase enzyme vestigial. This results in the production of an intermediate, termed 10-methylene stearate, which is detected only in S-type strains. Fatty acid methyl ester analysis of a C-type *Map bfaA* knockout revealed the loss of TBSA production, but the intermediate was present, similar to the S-type strains. Collectively, these results demonstrate the subtle biochemical differences between two primary genetic lineages of *Map* and other mycobacteria as well as explain the resulting phenotype at the genetic level. These data also suggest that TBSA should not be used as a diagnostic marker for *Map*.

IMPORTANCE Branched-chain fatty acids are a predominant cell wall component among species belonging to the *Mycobacterium* genus. One of these is TBSA, which is a long-chain middle-branched fatty acid used as a diagnostic marker for *Mycobacterium tuberculosis*. This fatty acid is also an excellent biolubricant. Control of its production is important for industrial purposes as well as understanding the biology of mycobacteria. In this study, we discovered that a carboxylic acid compound termed pivalic acid inhibits TBSA production in mycobacteria. Furthermore, *Map* strains from two separate genetic lineages (C-type and S-type) showed differential production of TBSA. Cattle-type strains of *Mycobacterium avium* subspecies *paratuberculosis* produce TBSA, while the sheep-type strains do not. This important phenotypic difference is attributed to a single-nucleotide deletion in sheep-type strains of *Map*. This work sheds further light on the mechanism used by mycobacteria to produce tuberculostearic acid.

KEYWORDS Johne's disease, tuberculostearic acid, fatty acid, *Mycobacterium*, pivalic acid

The species *Mycobacterium avium* comprises four genetically related subspecies that are diverse in phenotype and habitat niches (1). *Mycobacterium avium* subspecies *hominissuis* (*Mah*) causes disease in pigs and immunocompromised humans.

Mycobacterium avium subspecies *paratuberculosis* (*Map*) causes Johne's disease in ruminants, while *Mycobacterium avium* subspecies *silvaticum* (*Mas*) and *M. avium* subspecies *avium* may cause disease in birds. Within *Map* there are two primary phylogenetic clades designated C-type, also known as cattle type, and S-type, also known as sheep type, which are named for the hosts where they are primarily isolated. These two clades are further subdivided into three subtypes, with the S-type strains composed of subtypes I and III, while the C-type is exclusively subtype II (2, 3). All three subtypes are readily distinguishable using a variety of molecular typing methods (4–8). More distantly related to the *M. avium* subspecies is *M. smegmatis*, a fast-growing soil saprophyte that is a well-studied mycobacterial strain with a large repertoire of genetic and biochemical information (9). In this study, we examined the variability in fatty acid profiles produced by these mycobacteria in defined conditions.

The mycobacterial cell wall is unique among prokaryotes as it contains rare combinations of carbohydrate and lipid molecules such as lipoarabinomannan (LAM) and sulfated glycolipids. Notable differences in the cell wall lipids of *M. avium* subspecies have been documented. *Mah* and *Maa* produce glycopeptidolipids, whereas *Map* does not (10). Within *Map* itself, there are differences in the number of amino acids present in lipopeptides. The S-type strains produce a lipotripeptide, whereas the C-type strains produce a lipopentapeptide (6, 11). Fatty acids are another predominant structure of the mycobacterial cell wall. Originally, no differences in the fatty acid profiles were detected by gas chromatography/mass spectrometry (GC/MS) among 38 *M. avium* strains (12); however, more recently, differences have been noted even among *Map* C- and S-type strains (13). Furthermore, differences between C-type and S-type strains are not limited to cell wall lipids and fatty acids. The S-type strains generally grow slower and are more fastidious than C-type strains (14, 15), although this phenotype may be culture media dependent (2, 16, 17). C-type strains are more commonly isolated worldwide from a variety of ruminants (2, 18–21) and wildlife species (22). Only the C-type strains store iron when that mineral is in low abundance (23), and virulence adhesion differences in a heparin-binding protein have been observed between C-type and S-type strains (24) as well as other pathological differences (25). Genetically, large deletions in the S-type strains have been noted when compared to C-type *Map* (6, 26). In this study, we discovered another notable difference between C- and S-type *Map* in their production of branched-chain fatty acids linked to phospholipids.

Branched-chain fatty acids are not as common as straight-chain fatty acids but do occur in Gram-positive bacteria. A well-known example is *Streptomyces* production of tunicamycins, a secondary metabolite that is a branched-chain fatty acid with toxicity to prokaryotes and eukaryotes (27). Pivalic acid is a short chain-branched fatty acid with a tert-butyl group (28) that is a precursor for branched-chain fatty acid synthesis by several bacteria (29) and is used by *Streptomyces* as a substrate to produce tunicamycin (30). Palmitic, oleic, and tuberculostearic acids (TBSAs) are the predominant fatty acids in the surface phospholipids of mycobacteria (31). However, because palmitic and stearic acids are saturated fatty acids, only oleic acid is the most abundant unsaturated fatty acid in *Map* and other mycobacteria. Palmitic and tuberculostearic acids are ester linked to a triacylglyceryl compound (32, 33). In the current study, pivalic acid was used to control production of a branched-chain fatty acid in mycobacteria.

Most biological membrane samples contain long chain fatty acids. Tuberculostearic acid (10-methyloctadecanoic acid; TBSA) is a long branched-chain fatty acid linked to LAM in the cell wall of mycobacteria, where it comprises up to 20% of all fatty acids (34). TBSA decreases when *Mycobacterium phlei* is exposed to temperatures below 20°C (34). This same study also showed that mean fatty acid chain length and unsaturation increased in low temperatures, owing to the increase of oleic and linoleic acids. These observations suggest that TBSA, in concert with other fatty acids, actively regulates lateral membrane heterogeneity (35) and maintains membrane fluidity in colder temperatures (34). TBSA is also an ideal bio-based lubricant since the saturated fatty acid displays a low melting temperature (13.2°C) due to the methyl branch

occurring in the middle of the carbon chain as opposed to the more common iso and anteiso conformations (36). The biosynthesis of TBSA is a two-step process involving two enzymes and oleic acid as the substrate (37). These enzymes are BfaB, an S-adeno-syl-l-methionine-dependent methyltransferase, and BfaA, a flavin adenine dinucleotide (FAD)-binding oxidoreductase. Expression of these two mycobacterial genes is necessary and sufficient for production of TBSA in *Escherichia coli* (37) and as a two-gene fusion in yeast (36). An intermediate, termed 10-methylene stearate (C18:1 10-me), is formed in this two-step process. This intermediate is generally not detectable in *Mycobacterium* but has been observed in *Corynebacterium* species (38).

TBSA is considered a taxonomic and diagnostic marker for most *Mycobacterium* species (39), although it has also been identified in some *Corynebacterium* species (38). This marker is an excellent heat stable analytical target that can be readily detected in mouse lungs and is useful for anti-tuberculosis drug screening (40). The amount of TBSA has been strongly correlated to *Mycobacterium tuberculosis* growth measured by colony-forming units (CFUs) (40). This fatty acid is present in the fast-growing species *Mycobacterium smegmatis* (41) and *Mycobacterium phlei* (34, 42), as well as the slow-growing pathogenic species *M. avium*, *Mycobacterium leprae* (43), and most notably, *M. tuberculosis* (44). The only mycobacterial species that is not known to produce TBSA is *Mycobacterium gordonae* (44) due to the absence of TBSA biosynthetic genes (35). TBSA is incorporated in the lipids phosphoinositol, phosphoenthanolamine, and phosphoi-nositol manosides, which comprise the membrane phospholipids (39, 45). However, Alonso-Hearn and colleagues showed that *Map* does not always produce TBSA (13). Therefore, in this study, we investigated the factors that control TBSA production and uncovered a mechanistic difference unique to S-type strains of *Map*.

MATERIALS AND METHODS

Bacterial strains and growth conditions

M. smegmatis, *Map*, *Mas*, and *Mah* were all used in this study. *M. smegmatis* was cultured in tryptone yeast glucose (TYG) broth supplemented with Tween 80 (0.05%) at 37°C with shaking at 100 rpm. All *M. avium* subspecies cultures were incubated stagnant at 37°C. The media for *M. avium* subspecies cultures consisted of the Middlebrook 7H9 base with or without agar (1.5%) and Tween 80 (0.05% [vol/vol], Sigma-Aldrich) and Mycobactin J (2 mg/L, Allied Monitor). After autoclave sterilization at 121°C for 15 min and cooling to 50°C, the supplement, either oleic acid albumin dextrose catalase (OADC; Becton Dickinson) or albumin dextrose catalase (ADC; Becton Dickinson) was added to a final concentration of 10% (vol/vol). The only difference between these supplements was the presence of oleic acid. Sodium trimethylacetate hydrate (Sigma-Aldrich, catalog number 309591), referred herein as pivalic acid, was added to the growth media prior to autoclaving. *Map* was also cultured in BD BBL Herold's Egg Yolk Medium (HEYM) supplemented with amphotericin, nalidixic acid, vancomycin, and Mycobactin J (BBL catalog number B222233) and Lowenstein-Jensen 1-oz. bottle slants (Remel R10100, Thermo Fisher Scientific).

To set up concentration gradients, serial twofold dilutions of pivalic acid (0.125–32.0 mg/mL) were performed in a flat-bottomed 96-well plate with 7H9 broth supple-mented with OADC, Tween 80, and Mycobactin J for *M. avium* strains and in TYG supplemented with Tween 80 for the *M. smegmatis* strain. Control wells were pivalic acid free to serve as either a (growth control, with mycobacteria) or sterility control (no mycobacteria). After the addition of pivalic acid (except for the control wells), 100 µL of a mycobacterial suspension at an optical density at 600 nm (OD_{600}) = 0.02 containing 10^6–10^8 CFU/mL was added to each well. Plates were incubated for 5 days (*M. smegmatis*, *Mah*, and *Ma* strains) or 17 days (*Map* and *Mas* strains) at 37°C–39°C, protected from light. The optical density of all cultures was measured at 600 nm. The percentage of growth inhibition was calculated as percent inhibition = $1 - [(OD_{sample} - OD_{neg}) / (OD_{GC}$

– OD$_{neg}$)] × 100. *M. smegmatis* growth curves were measured on a Bioscreen C machine (Growth Curves USA) using 96-well honeycomb-style plates.

Minimal inhibitory concentrations (MICs) were determined using the resazurin microtiter assay. After incubation, 30 uL/well of resazurin was added, and the plates were incubated for another 4–24 h. Resazurin is a redox indicator that changes color (from blue/purple to pink) as bacteria consume O$_2$, allowing growth to be quantified. The MIC was defined as the lowest pivalic acid concentration preventing color change.

FAME esterification

The lipid extractions were performed in two ways: either by mini extraction (1-mL culture volume) or by larger extraction (100-mL culture volume). Mycobacterial cultures were harvested by centrifugation (1,000 × *g*, 10 min). The pellets were acidic Bligh-Dyer extracted with methanol-chloroform (1:1 by volume) in the presence of a catalytic amount of concentrated hydrochloric acid (2% [vol/vo]l). After vortex mixing to extract the cellular lipids, the extracts were clarified by centrifugation and dried on an airline. The residues were re-constituted in methanol:chloroform:HCl (500:500:20 µL) and heated in a sealed tube at 60℃ for 1 h to form fatty acid methyl esters (FAMEs). After cooling, the solutions were back-extracted with water (1 mL) to remove residual acid, and the chloroform layers were analyzed by electron impact gas chromatography/mass spectrometry (EI GC/MS). For some experiments, the FAME samples were reduced with 10-mg/mL sodium borohydride (borodeuteride) and re-analyzed by GC/MS.

Gas chromatographic mass spectrometry

The extracted lipid fractions were analyzed as FAMEs and as pyrrolidine derivatives using established EI GC/MS analytical procedures as described previously (27). The GC/MS analysis of the cellular FA derivatives was achieved in positive ion detection mode on a Shimadzu QP-2010 Plus instrument with autoinjector (Shimadzu Scientific Instruments, Addison, IL, USA). The GC column used was a Zebron ZB-1 capillary (30 m, 0.25 mm) with helium carrier (18.6 mL/min). A linear oven gradient was used from 150℃–250℃/4℃/min. Detector/interface and injector were maintained at 300℃ and 275℃, respectively. Quantitation of FAMEs was done by measuring peak area and normalizing against the largest internal peak (palmitic acid). Data are reported as a percentage of total peak area. Mass spectra were recorded and analyzed using Shimadzu GCMS Solution software.

Electron microscopy

Preparation of mycobacterial samples for transmission microscopy has been described previously (46). All mycobacteria were cultured in Middlebrook 7H9 for 60–80 days prior to fixation. Fresh media were added to cultures every 25 days to maintain steady-state growth. The fixation and staining procedures were conducted at room temperature. Cells were fixed overnight in 2.5% glutaraldehyde: 0.1 M cacodylate buffer, pH 7.4. Fixed cells were washed in the same buffer three times and were post-fixed in 1% OsO$_4$ in 0.1 M cacodylate buffer, pH 7.4, for 1 h. After washing in the same buffer, cells were incubated with 30% ethanol for 10 min. The cells were further dehydrated with a graded series of ethanol and embedded in epoxy resin (Embed 812). Ultrathin sections for electron microscopy were obtained and stained with uranyl acetate and Reynolds lead citrate and then observed under a Tecnai G2 Spirit BioTWIN electron microscope.

Genome and PCR product sequencing

M. smegmatis was sequenced on Illumina and assembled using MIRA, v. 4.9.6. This whole-genome shotgun project has been deposited at DDBJ/ENA/GenBank under accession number NZ_JALHLC010000018. The version described in this paper is v.NZ_JALHLC010000018.1. The BioProject accession number is PRJNA821894. PCR products to be sequenced were cleaned up using QIAquick PCR purification kits (Qiagen)

Knockout construction of *bfaA*

The ORBIT method was used for knockout construction of *Map* K-10 (47). This process involved consecutive electro-transformations of two plasmids, pKM444, which is kanamycin resistant, followed by pKM464, which is hygromycin resistant. The second electroporation with pKM464 also included the 168-bp oligonucleotide used to create the knockout (Fig. S1A). This process allows *oriE* and the hygromycin cassette in pKM464 to integrate in place of the target gene, making it hygromycin resistant (Fig. S1B). The pKM444 plasmid is lost after several passages, but the hygromycin cassette is maintained. Reverse transcription PCR (RT-PCR) was conducted using the Maxima SYBR Green/ROX real-time PCR assay (Thermo Fisher Scientific) according to the manufacturer's instructions to verify transcript presence or absence in the parent and knockout strains. Primers used to confirm the mutants and for RT-PCR to detect the presence of transcripts are shown in Table S1 and Fig. S1C.

Transcriptomics of *bfaA* and *bfaB*

Ten replicate RNA extractions were performed on *Map* K-10 cultured in Middlebrook 7H9 media supplemented as described above at 37°C for 20 days to achieve log phase. All RNA samples were evaluated on a BioAnalyzer (Agilent). RNA-seq data were obtained on an Illumina HiSeq3000 instrument to obtain 100-bp stranded single-direction reads. Reads were mapped to the *Map* K-10 genome sequence. Those reads that mapped to the entire 45-bp length of the intergenic region between MAP_0320 (*bfaA*) and MAP_0321 (*bfaB*), as well as reads mapping to any part of this region, were compiled and normalized to account for variations in read depths between samples. Reads were nomalized by reads per million mapped reads and reads per kilobase per million mapped reads. The BioProject ID associated with all the RNA-seq data is PRJNA1074775.

SNP analysis of *Map* C- and S-type strains

Sequence reads were extracted from the National Center for Biotechnology Information (NCBI) database using *Map* K-10 *gyrA* and *B*, as well as *bfaA* genes to query the reads. Single-nucleotide polymorphisms (SNPs) were inferred in FreeBayes (48), which created the variant call format files. Phred-scaled quality score for the assertion was made in ALT, i.e., −10log10 prob (call in ALT is wrong). If ALT is "." (no variant), then this is −10log10 prob(variant), and if ALT is not "", this is −10log10 prob(no variant). High-quality scores indicate high-confidence calls.

Statistical analysis

For FAME peak heights, arcsine transformation of FAMEs proportions was performed. Normality and homogeneity of variances were checked after transformation, and statistical analysis was performed using two-way analysis of variance and Šídák's or Tukey's post-test.

RESULTS

Map strain typing

To correlate TBSA production with the two primary phylogenetic clades of *Map* (C-type and S-type strains), genotyping was conducted to define the SNPs present in the *gyrA* and *gyrB* genes as described by Castellanos et al. (5). This method enabled us to categorize our own isolates (Table 1) as well as those present in public sequence databases. From this analysis, one of our sheep isolates (6094) was obtained from a Rambiollet breed but was found to be C-type; likewise, a second sheep isolate (6093) was obtained from a Polypay and was also C-type (Table 1). These results demonstrate

TABLE 1 Mycobacterial strains used in this study[a,b]

Species	Subspecies	Strain	Date	Map type	Subtype	Host
avium	*paratuberculosis*	K-10		C-type	II	Bovine
avium	*paratuberculosis*	6093	1 May 2004	C-type	II	Ovine
avium	*paratuberculosis*	6094	1 May 2004	C-type	II	Ovine
avium	*paratuberculosis*	S397	7 October 2004	S-type	III	Ovine
avium	*paratuberculosis*	S467	7 October 2004	S-type	III	Ovine
avium	*paratuberculosis*	ATCC19698		C-type	II	Bovine
Aavium	*hominissuis*	6092		N/A	N/A	
avium	*hominissuis*	09-4418	25 February 2011	N/A	N/A	Swine
avium	*hominissuis*	09-4407	25 February 2011	N/A	N/A	Bovine
avium	*hominissuis*	MAC104	28 April 2004	N/A	N/A	Human
avium	*avium*	MA1025	12 November 2004	N/A	N/A	Gazelle
avium	*silvaticum*	ATCC49884		N/A	N/A	Wood pigeon
smegmatis		mc^{2}155		N/A	N/A	N/A

[a]ATCC, American Type Culture Collection; N/A, not applicable.
[b]The date denotes the date isolated, if known.

that C-type strains, typically isolated from cattle, can also be obtained from sheep in the United States. This phenomenon has also been reported in Canada (15) but is generally considered rare. Including sequences extracted from public sequence databases, a total of 509 strains were C-type and 72 strains were S-type, of which 64 strains were further divided into subtype I and eight strains were subtype III.

Growth of mycobacteria in pivalic acid is inhibitory

Several bacteria use pivalic acid as a primer unit for the biosynthesis of *tert*-butyl fatty acids (28, 49). Pivalic acid stimulated the growth of *M. smegmatis* at low-dose concentrations (0.5–1.0 mg/mL) but then became inhibitory as concentrations increased to 2.5 mg/mL and above (Fig. 1A). Repeated experiments confirmed that stimulatory concentrations of pivalic acid on *M. smegmatis* growth were significant at 0.5 mg/mL after 36 h of growth (Fig. 1B). *M. avium* subspecies were more sensitive to pivalic acid with two *Mah* strains (MAC104 and 09–4407) showing growth inhibition at 0.12 mg/mL, while the MA1025 and *Mah* 09–4418 strains showed marginal growth stimulation at that same concentration (Fig. S2A). *Mas* and *Map* were more sensitive to pivalic acid reaching a 90% growth inhibition at 8 mg/mL (Fig. S2A and B). The MIC was next determined for all strains by optical density (Table 2) and resazurin (Fig. S3). Both experiments show *M. smegmatis* is least sensitive to pivalic acid, while *Map* strains and *Mas* are most sensitive. In summary, pivalic acid is inhibitory with *M. avium* strains, but the MICs vary among strains. Also, low concentrations of pivalic acid resulted in pronounced stimulatory growth of *M. smegmatis* with an inhibitory effect observed only at higher concentrations.

Pivalic acid affects cellular fatty acid production in mycobacteria

Mycobacterium produces several cellular fatty acids with palmitic acid as the predominant straight-chain fatty acid when FAMEs are extracted and analyzed by GC/MS (Fig. 2A). However, higher levels of palmitic acid are observed in all strains compared to the C-type *Map* strains. FAME extracted *Map* cultured in Middlebrook 7H9 media with and without pivalic acid reveals six major peaks at 8.3 min (C14:0, myristic acid), 11.3 min (C16:1, palmitoleic acid), and 11.7 min (C16:0, palmitic acid), and three C18 peaks in the region of 14.4–16.2 min, the last of which is the mid-chain methyl-branched fatty acid TBSA at 15.9 min (Fig. 2B and C). However, the addition of 0.5-mg/mL pivalic acid to C-type *Map* cultures inhibited TBSA production as shown by the missing peak at 15.9 min in the top trace of Fig. 2B and C. Palmitoleic acid (C16:1), which is synthesized by desaturation of palmitic acid, was also inhibited by pivalic acid (Fig. 2B; Table 3).

Furthermore, when *Map* was cultured in increasing concentrations of pivalic acid, inhibition of myristic and oleic acid production was observed in addition to TBSA
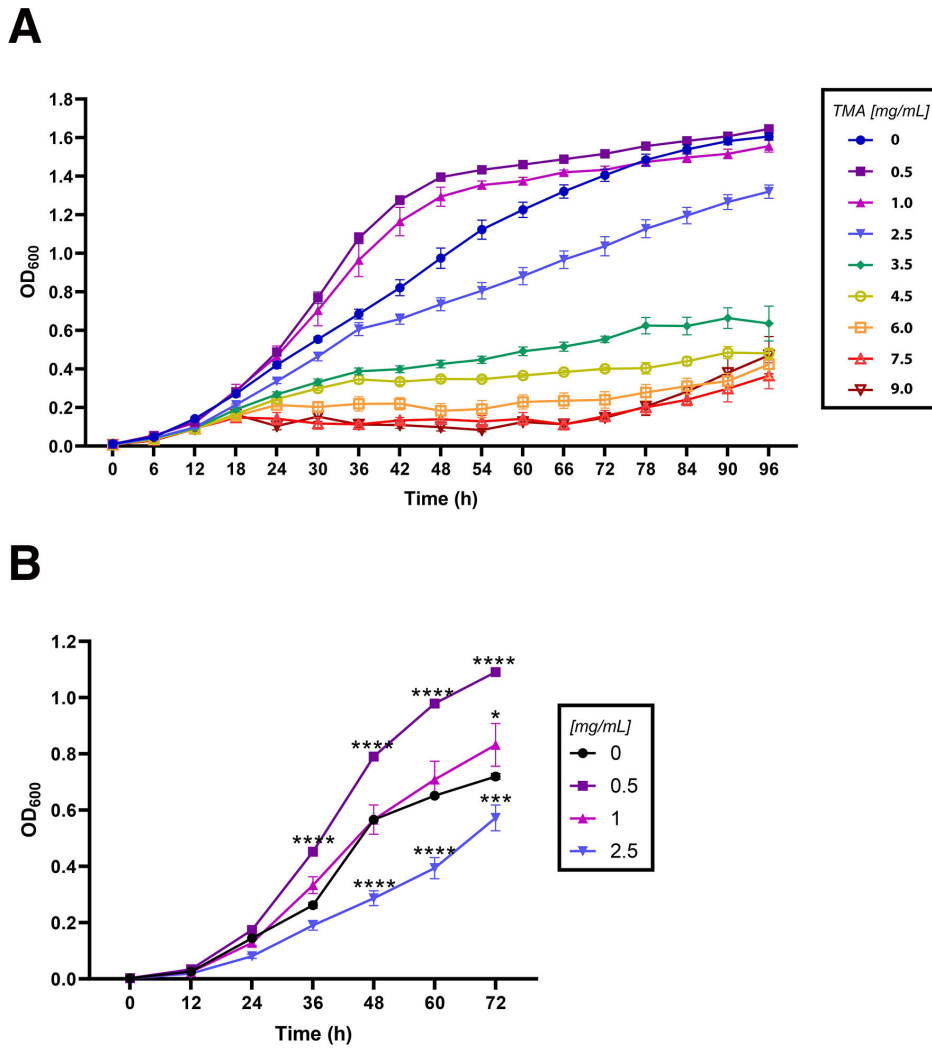
FIG 1 Growth of *M. smegmatis* is stimulatory at low concentrations of pivalic acid and inhibitory at higher concentrations. (A) *M. smegmatis* growth at 37°C in TYG-Tween 80 was measured every 6 h by optical density at 600 nm in concentrations ranging from 0.5 to 9.0 mg/mL ($n = 3$). The data are expressed in mean (OD_{600}) ± SEM. (B) Growth curve of *M. smegmatis* in low concentrations of pivalic acid ($n = 6$). Growth at 37°C in TYG-Tween 80 was measured every 12 h by optical density at 600 nm. The data are expressed in mean (OD_{600}) ± SEM. Significant differences compared to the 0-mg/mL concentration at each time point were determined using two-way analysis of variance and Tukey's post-test. *$P < 0.05$, ***$P < 0.001$, ****$P < 0.0001$. SEM, standard error of the mean.

(Fig. 3A and B; Table S2). This was not observed in non-*Map* strains (Fig. 3C and D; Table S2). Conversely, there is a buildup of stearic acid which occurs whether analyzed by total ions or mass-to-charge ratios (Table 3). Middlebrook 7H9 media itself, contains oleic, palmitic, and stearic acid peaks (Table S3). Only FAMEs from *M. smegmatis* are not affect by increasing concentrations of pivalic acid up to 4.5 mg/mL (Fig. 3D). Myristic, palmitic, oleic, and stearic acids are detected at similar levels in other *M. avium* subspecies including *hominissuis* and *silvaticum* (Fig. 3C; Table S4). However, TBSA is still produced in those non-*Map* subspecies at 0.5-mg/mL pivalic acid. Fatty acid profiles from these subspecies also produce the expected myristic, palmitic, oleic, and stearic acids when cultured in Middlebrook 7H9 without pivalic acid (Fig. 2A). Furthermore, the fatty acid profiles from *Mah* also show a dose-dependent effect as TBSA and myristic acid production is reduced when the concentration of pivalic acid increases (Fig. 3C; Table S2). Specifically, production stops at 2.5-mg/mL pivalic acid for *Mah* and at 0.5 mg/mL for

TABLE 2 Pivalic acid MIC results on mycobacteria

Strain	Pivalic acid (mg/mL)
M. smegmatis	>32
Ma MA1025	32
Mah MAC104	32
Mah 09-4407	32
Mah 09-4418	32
Mas ATCC49884	4–8
Map K10	8
Map ATCC19698	4
Map 6094	16
Map S467	8
Map ΔMAP_0320	4–8

Map (Fig. 3A through C; Table S2). The other notable difference with *Mah* FAMEs is that oleic acid does not decrease when pivalic acid increases.

This dose-dependent effect was also observed for *M. smegmatis*; however, the concentration of pivalic acid needed to inhibit TBSA production is much higher (>5 mg/mL) than what was observed with the slow-growing mycobacteria. Although no *M. smegmatis* fatty acid changes were evident in the concentration range shown in Fig. 3D, TBSA does decrease as pivalic acid concentration increases above 4.5 mg/mL (Table 4). Collectively, these data suggest that pivalic acid is being incorporated into cellular fatty acids and controls the amounts of specific fatty acids, which influence growth rate.

The S-type strains of *Map* do not produce TBSA regardless of the presence of pivalic acid

While C-type *Map* and non-*Map* strains produce TBSA when cultured without pivalic acid, the *Map* S-type strains do not make TBSA in any growth condition. Instead, they produce 10-methylene-stearate, which is essentially TBSA with a 9,10-double bond and is distinguishable by GC/MS (Fig. 2A; Fig. S4). This compound is the intermediate in TBSA biosynthesis with oleic acid as the substrate (Fig. S5). *Map* S467, another S-type strain, also produces the same intermediate with no TBSA detectable (Fig. S4B).

Although these S-type strains make only the intermediate, production of this compound stops at or above 0.5-mg/mL pivalic acid with both S-type strains tested (Fig. 3; Fig. S4B). Myristic acid and oleic acid also stop production at 0.5 mL/mL pivalic acid (Fig. S4B). Stearic acid and palmitic acid increase from ~5% to 38% at the point where C18:1 10-me production stops (from 12% down to 0%) (Table S2; Fig. S4B). This is different from the C-type strains, which continue producing oleic acid when cultured in pivalic acid above 0.5 mg/mL (Fig. 3A; Table S2). To demonstrate that host origin is not a determining factor for TBSA production, two C-type isolates previously obtained from independent breeds of sheep produced TBSA (Table S5). Overall, pivalic acid is inhibiting growth, and this correlates with reduced conversion of stearic acid to oleic acid, along with the subsequent conversion of oleic to TBSA in C-type strains or 10-methylene stearate in the S-type strains.

Sodium borohydride reduction converts the 10-methylene stearate intermediate to TBSA

To confirm the structure of the intermediate, FAME extracts from an S-type strain were reduced with sodium borohydride. S-type strains produce the 10-methylene-stearate intermediate, which can be reduced by the borohydride to 10-methyl-stearate or TBSA. Furthermore, the compound was reduced to 10-(deutrero)-methyl-stearate with the borodeuteride (Fig. 4A). Essentially, the double bond in the 10-methylene (−CH = CH2) is reduced to 10-methyl (−CH2−CH3), converting the intermediate into TBSA. EI GC/MS was used to ionize and fragment analyte molecules present in the C18 peaks before mass spectrometric analysis and detection to confirm the intermediate conversion to
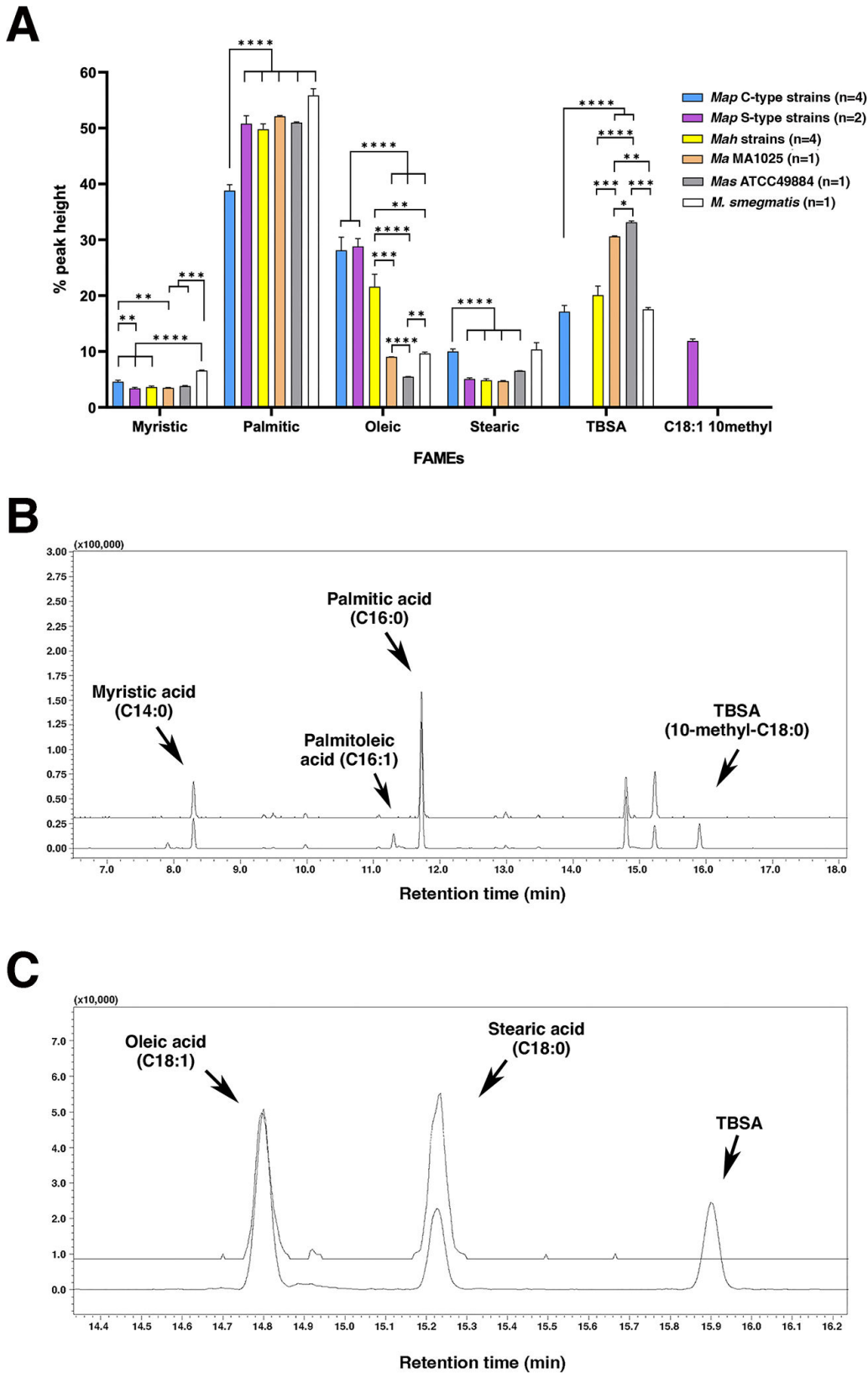
FIG 2 GC/MS analysis of FAME extracted mycobacteria with and without pivalic acid. (A) Quantitative fatty acid peak areas for *Mycobacterium* strains cultured in the absence of pivalic acid as analyzed by GC/MS. Data are the mean percent of peak area ± standard error of the mean (repeated at least twice). Normality and homogeneity of variances were checked, and statistical

FIG 2 (Continued)

analysis was performed using two-way analysis of variance and Šídák's post-test. *P < 0.05, **P < 0.01, ***P < 0.001, ****P < 0.0001. (B) In *Map*, six primary fatty acid peaks are separated by GC/MS at 8.3 min (C14:0), 11.3 min (C16:1), 11.7 min (C16:0, palmitic—the largest peak), then three C18 peaks spanning the region at 14.4–16.2 min. (C) Expanded region from 14.4 to 16.2 min of the spectra in panel B. The C18 peaks are 14.8 min (C18:1), 15.25 min (C18:0), and 15.9 min (TBSA, 10-methyl-C18:0), the latter of which is absent in cells cultured in 0.5-mg/mL pivalic acid. In both panels B and C, the top trace is FAME extracted *Map* cultured in 0.5-mg/mL pivalic acid and the bottom trace is *Map* cultured without pivalic acid. The *y*-axis is fatty acid peak height.

TBSA after sodium borohydride reduction (Fig. S6). This method provided a structural confirmation of the compounds. Fatty acid pyrrolidide derivatives were also generated and provided independent corroboration of these fatty acid structures, which resulted in cleaner GC/MS profiles than the sodium borohydride reduction (Fig. 4B). These pyrrolidide derivatives were likewise confirmed by EI GC/MS (Fig. S7). Both experiments independently confirm these compounds are the 10-methylene stearate intermediate observed only in S-type strains.

TBSA is produced in a variety of growth conditions

Map is typically cultured in Middlebrook 7H9 media supplemented with OADC, while many other mycobacterial species, including *M. smegmatis*, grow in ADC supplemented cultures. The difference in these two supplements is oleic acid. Oleic acid is a substrate fatty acid for the conversion to tuberculostearic acid (Fig. S5). Two strains of *Map* were cultured in Middlebrook 7H9 broth supplemented with OADC and with ADC for 5 weeks. There was no significant difference in *Map* growth rate when cultured in OADC- or ADC-supplemented media (Fig. 5), demonstrating the presence of oleic acid in the medium is not a requirement for growth. FAME analysis of these cultures showed TBSA production regardless of the supplement used (Table 5), suggesting that exogenous oleic acid is not required to produce TBSA. Likewise, TBSA was produced when *Map* C-type was cultured in HEYM and Lowenstein-Jensen media (Table 5), but S-type *Map* did not produce TBSA and only low or undetectable levels of the intermediate (C18:1 10-me) when cultured in Lowenstein-Jensen media (Table 5). The intermediate was also not detected in S-type *Map* grown in HEYM media. *Map* cultured in 5% CO_2 with and without pivalic acid for 67, 75, and 95 days again shows an inhibitory effect on TBSA production but also stops myristic and palmitoleic production as before (Table S6). Collectively, these data suggest that TBSA production is relatively stable in different conditions. Also, 10-methylene stearate production in the S-type strains was not produced in HEYM cultures.

Genomic organization of *bfaA* and *bfaB* genes in *M. avium* subspecies

We have shown that two S-type strains of *Map* did not produce TBSA regardless of the presence or absence of pivalic acid or other growth conditions tested. Other investigators have observed this same lack of TBSA production in another S-type strain (13).

TABLE 3 Comparison of *Map* FAME total ions versus mass-to-charge ratios[a]

| Retention time | Ions | Fatty acid | Total ions | | *m/z* 74 ion extraction | |
			0 pivalic[b]	0.5 pivalic	0 pivalic	0.5 pivalic
8.296	C14:0	Myristic	5.85	6.50	12.73	10.95
11.304	C16:1	Palmitoleic	12.51	0.00	0.00	0.00
11.722	C16:0	Palmitic	23.00	29.19	49.17	49.87
14.798	C18:1	Oleic	44.84	50.76	18.87	17.61
15.225	C18:0	Stearic	5.07	13.55	9.66	21.57
15.901	C18:0M	TBSA	8.73	0.00	9.58	0.00

[a]Quantitative GC/MS: total ions or mass-to-charge (*m/z*) 74 ion extraction.
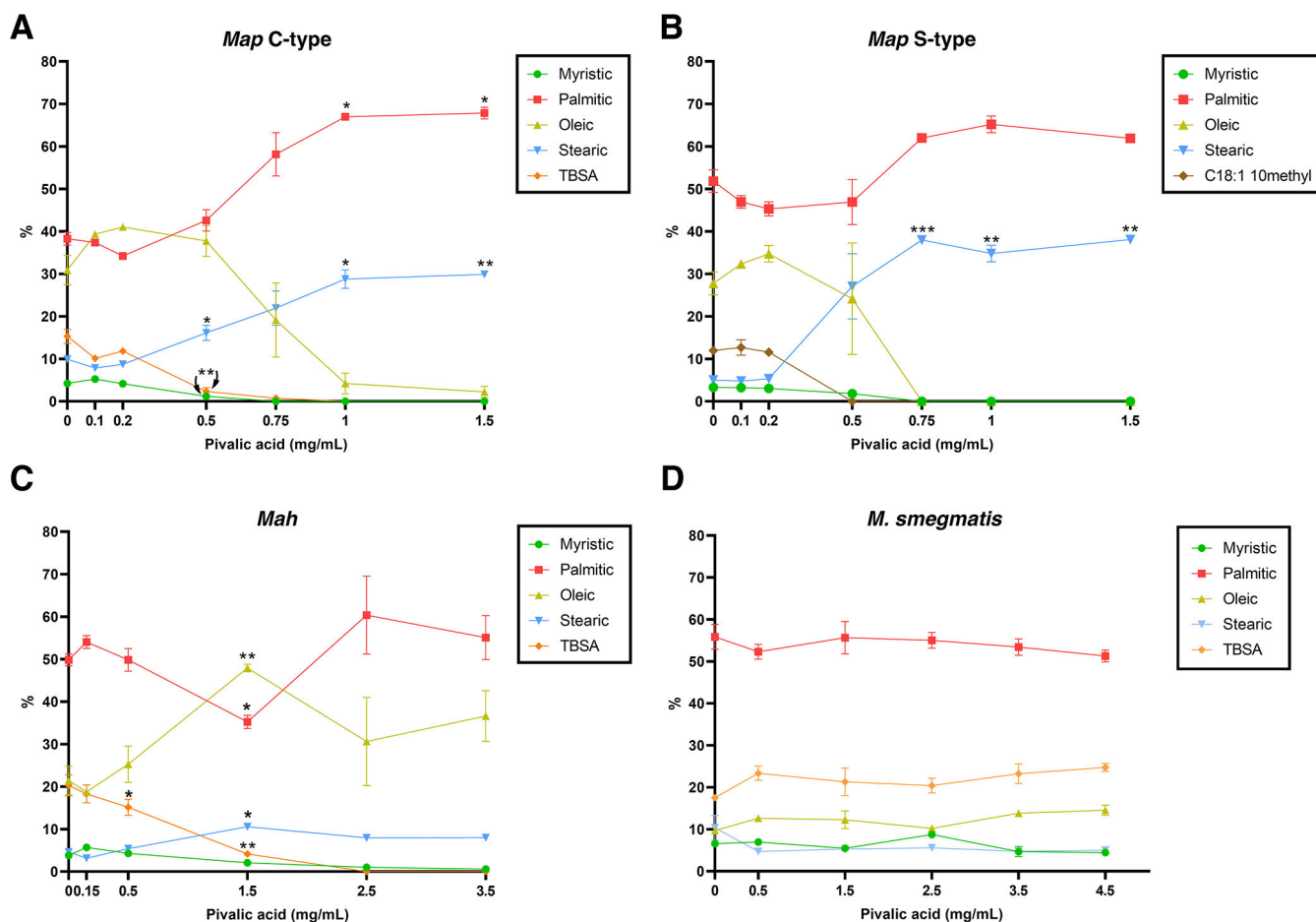[b]0 pivalic and 0.5 pivalic are in mg/ml.

FIG 3 Pivalic acid affects *M. avium* subspecies fatty acid production. Shown are the quantitative FAME results from C-type (A) and S-type (B) strains of *Map*, along with *Mah* (C) and *M. smegmatis* (D). Data are expressed as the mean peak area percent with SEM. For statistical analysis, arcsine transformation of FAME proportions was performed. Normality and homogeneity of variances were checked, and statistical analysis was performed using two-way analysis of variance and Šídák's post-test. Significant differences compared with no pivalic acid are *$P < 0.05$, **$P < 0.01$, ***$P < 0.001$.

The genes encoding BfaA and BfaB have been shown to convert oleic acid to TBSA in *M. tuberculosis* (33) via a two-step biosynthesis (Fig. S5). The *bfaA* and *bfaB* genes are arranged in tandem on all *M. avium* subspecies chromosomes in a manner consistent with *M. smegmatis* (Fig. S8). To determine if these genes are co-transcribed in a single operon, transcriptomics analysis of C-type *Map* was performed and confirmed what was predicted previously for *M. smegmatis* (35) that both genes are co-transcribed in a single polycistronic mRNA on the leading strand as shown by mapped reads that span the intergenic region in 10 stranded single-direction RNA-Seq samples (Table S7).

TABLE 4 High-dose effect of pivalic acid on *M. smegmatis* TBSA production[a]

Pivalic acid (mg/mL)	Palmitic C16:0 11.70 min	Oleic C18:1 14.77 min	Stearic C18:0 15.19 min	Tuberculostearic C18:0 10-methyl 15.87 min
0	49.92	18.19	11.08	20.81
4.5	46.65	18.73	19.16	15.46
6.0	47.86	19.8	19.23	13.11
9.0	51.43	15.3	26.71	6.57

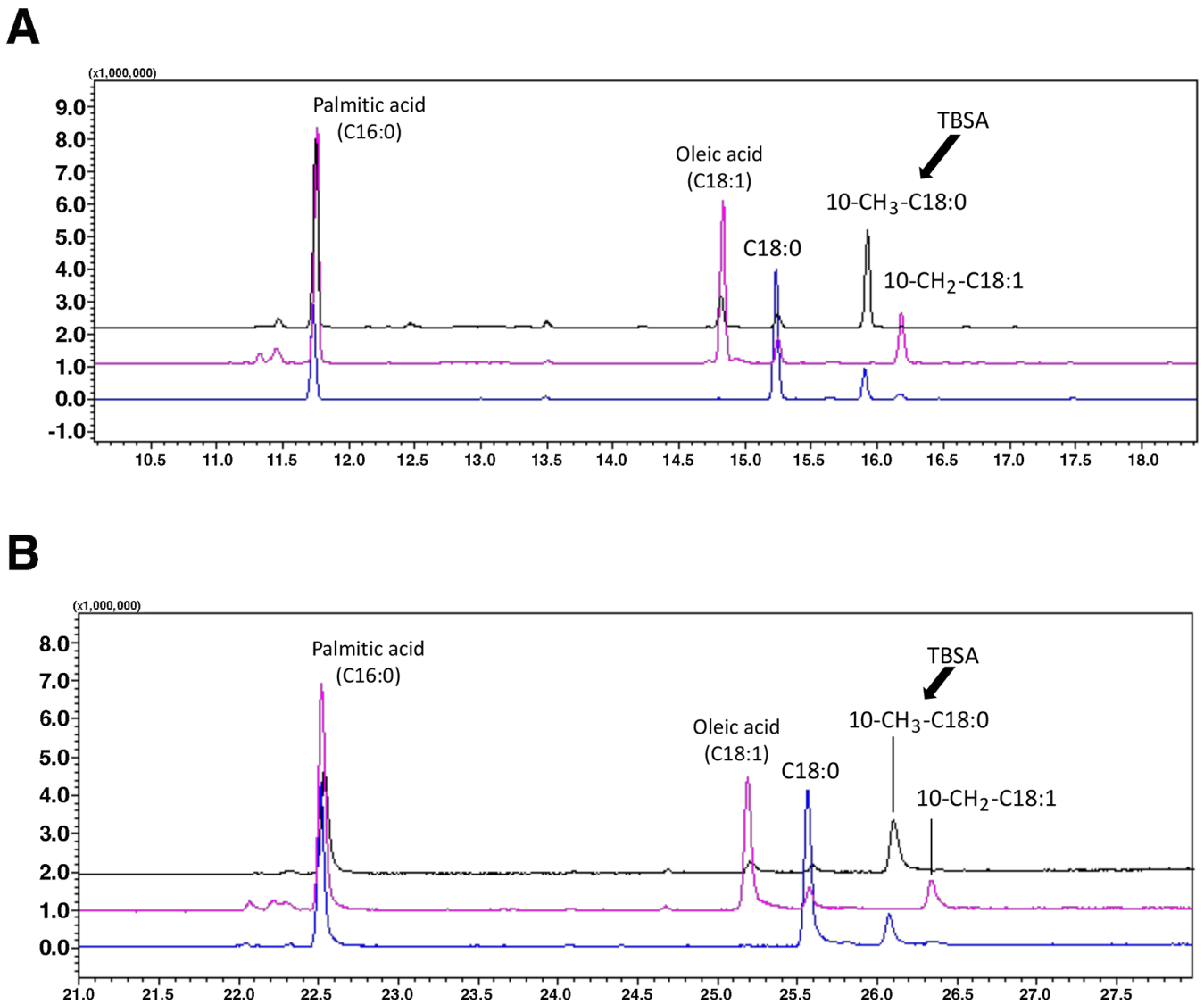[a]Data are reported as percentage of total peak height.

A

B

FIG 4 Structure confirmation of the 10-methylene-stearate compound in the S-type strain *Map* S397. Two approaches were used to confirm the intermediate structure, sodium borohydride reduction of the intermediate (A), and fatty acid profiles as pyrrolidine derivatives (B). (A) GC/MS pileup scan of FAME extracted S397 samples that were reduced with sodium borohydride (blue trace) or not reduced (pink trace). *Mah* (black trace) was used as a control showing the location of TBSA. Note that after reduction with sodium borohydride, the TBSA peak is observed, indicating the intermediate was reduced to TBSA in the S-type strain. (B) Pyrrolide analysis of the intermediate produced by S397. Note the intermediate (10-CH2-C18:1) is produced only in S397, not *Mah*. However, *Mah* produces 10-CH3-C18:0 (TBSA) as shown by the peak at 26.1 min. After NABH4 treatment, the 10-CH2-C18:1 is reduced to 10-CH3-C18:0. The oleate is also reduced to stearate. This confirms the assignment of the 26.34-min GC peak as 10-methylene-stearate.

One SNP is responsible for lack of TBSA production in S-type strains

Alignment of the *bfaA* gene in all *M. avium* subspecies shows an SNP that is only present in S-type strains (Fig. 6A). This SNP results in a frameshift and premature stop codon, which produces a truncated and non-functional BfaA protein of 400 amino acids (Fig. 6B). K-10 produces the full-length BfaA protein comprising 474 amino acids (Fig. 6B). SNP analysis of additional *Map* strains shows the same frameshift mutation occurs in all S-type strains, while all 509 C-type strains encode the full-length protein (Table S8). Genomic analysis indicates all other *M. avium* subspecies examined, except S-type *Map*, have the full-length gene. In total, all 72 S-type strains analyzed were positive for the *bfaA* SNP (64 subtype I and eight subtype III). In contrast, the *bfaB* gene sequence is 100% conserved across all *Map* types. These data suggest the mechanism for explaining
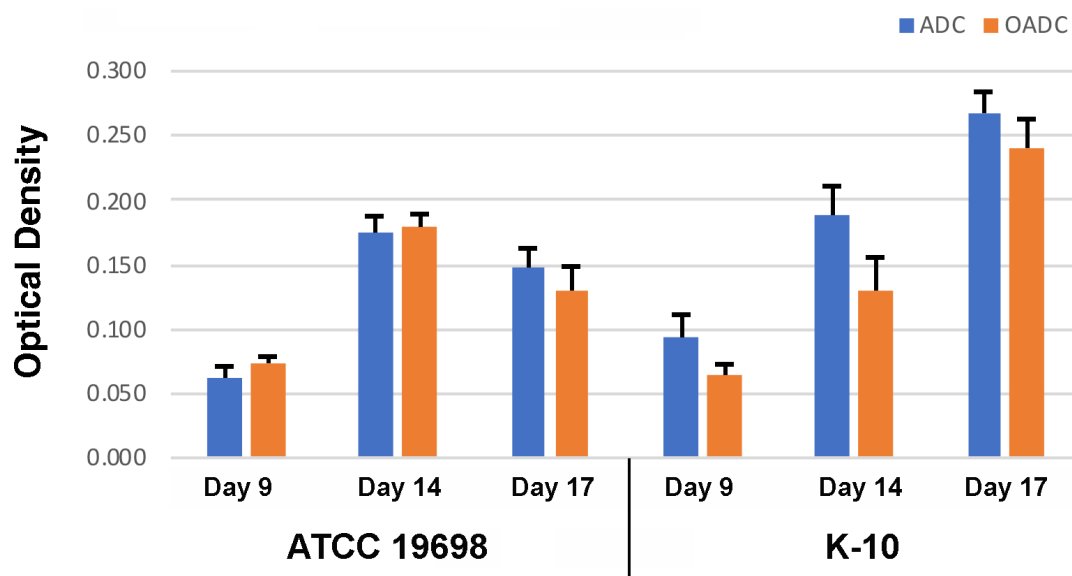
FIG 5 The presence of oleic acid in culture media is not required for growth of two C-type *Map* strains. the ATCC19698 and K-10 strains were cultured for 17 days in Middlebrook 7h9 with either ADC or OADC supplement. Optical density measurements were taken in triplicate, and error bars represent standard errors of the mean.

production of 10-methylene stearate but not TBSA in S-type strains. A shotgun genome sequence was conducted on the *M. smegmatis* strain used in this study to determine the presence of *bfaA* and *bfaB* gene SNPs. Illumina reads were assembled and show that *bfaA* and *bfaB* genes are present in this strain (Fig. S8). Alignment of these genes with another *M. smegmatis* strain in NCBI (FOB87_RS25320 and FOB87_RS25325, respectively, in *M. smegmatis* FDAARGOS_679) shows identical sequence with no polymorphisms.

Construction of a *bfaA* (ΔMAP_0320) knockout in *Map* K-10

Our hypothesis is that a *bfaA* knockout in the C-type strain K-10 will produce 10-methylene stearate instead of TBSA (10-methyl-stearate). The gene-deletion mutant was constructed using the oligo-based ORBIT system, which uses two plasmids and an oligonucleotide to create the knockout (Fig. 7A) (47). Two independent ΔMAP_0320 mutants were identified in a DNA amplification screen and designated C4 and C10 (Fig. S9). Transcripts of ΔMAP_0320 were not detected in either of these mutants, which confirmed the gene ablation (Fig. 7B). We also attempted the same construction in *Mah*. However, despite three independent attempts, no colonies were obtained as this subspecies appears to be more resistant to electro-transformation of DNA or targeted mutagenesis compared to *Map*.

The ΔMAP_0320 knockout has a GC/MS profile similar to S-type strains

GS/MS analysis of the C-type ΔMAP_0320 knockouts showed no production of TBSA but only the 10-methylene stearate intermediate (Fig. 8A). The wild-type strain harboring the pKM444 plasmid used in constructing the knockout showed a GC profile that was similar to the C-type strains. EI GC/MS confirmed the intermediate structure produced by the knockout (Fig. 8C) and TBSA produced by the control *Map* harboring only the pKM444 plasmid (Fig. 8B). These results confirm the essential role of the FAD-binding oxidoreductase in TBSA production.

TABLE 5 Quantitative FAME analysis of *M. avium* subspecies cultured in different media and conditions[a]

Subspecies	Strain	Growth (days)	Media/condition	Palmitic C16:0	Oleic C18:1	Stearic C18:0	TBSA C18:0 10-me	C18:1 10-me
paratuberculosis	K10	17	ADC	23.28	61.12	3.17	12.45	–
paratuberculosis	K10	17	OADC	24.41	55.14	4.37	16.09	–
paratuberculosis	ATCC19698	17	ADC	29.05	50.57	4.17	16.22	–
paratuberculosis	ATCC19698	17	OADC	26.12	53.58	5.69	14.61	–
paratuberculosis	K10	28	HEYM	52.38	20.82	20.02	6.79	–
paratuberculosis	K10	30	Lowenstein-Jensen	53.90	14.62	25.35	6.13	–
paratuberculosis	K-10	151	Lowenstein Jensen	50.61	24.82	14.28	10.28	–
paratuberculosis	S397	76	HEYM	48.29	24.59	27.12	–	–
paratuberculosis	S397	30	Lowenstein-Jensen	44.97	36.25	17.18	–	1.60
paratuberculosis	S397	151	Lowenstein Jensen	50.09	25.26	24.65	–	–
paratuberculosis	S467	64	HEYM	44.85	32.14	23.01	–	–
paratuberculosis	S467	64	Lowenstein-Jensen	53.85	13.92	32.23	–	–
hominissuis	6092	30	HEYM	59.24	20.22	14.56	5.98	–
hominissuis	6092	28	Lowenstein-Jensen	54.23	17.93	10.61	17.24	–
hominissuis	6092	111	Lowenstein-Jensen	41.42	46.99	9.72	1.87	–
hominissuis	6130	28	HEYM	65.97	5.00	18.57	10.46	–
hominissuis	6130	28	Lowenstein-Jensen	53.87	18.19	16.87	11.06	–
hominissuis	6130	111	Lowenstein-Jensen	44.41	43.32	10.16	2.10	–
paratuberculosis	6093	28	HEYM	55.05	19.38	18.64	6.92	–
paratuberculosis	6093	30	Lowenstein-Jensen	41.48	36.46	16.99	5.07	–
paratuberculosis	ATCC19698	30	HEYM	55.47	18.41	22.91	3.22	–
paratuberculosis	ATCC19698	28	Lowenstein-Jensen	55.94	17.84	20.87	5.35	–
paratuberculosis	ATCC19698	151	Lowenstein-Jensen	51.55	20.57	26.50	1.38	–
paratuberculosis	6094	151	Lowenstein-Jensen	45.93	30.54	22.28	1.26	–

[a]Data are reported as percent of total peak area.

The *bfaA* knockout is morphologically similar to K-10 and S397

Because TBSA is a predominant fatty acid in mycobacterial surface phospholipids, the wild-type and knockout strains of *Map* were examined by transmission electron microscopy to determine if any morphological differences were detectable. Ultra-thin sections of the bacteria all showed variable shapes in each field, depending on how the bacteria were arranged in the paraffin block (Fig. S10). No differences were observed between S397, K-10, or the knockouts at ×13,000 magnification or ×30,000 magnification (Fig. S10). Cells were also examined at ×68,000 with no detectable differences. Likewise, growth rate differences between the knockouts and wild-type were not significant.

DISCUSSION

Both pivalic acid and a *bfaA* mutation can prevent TBSA production in *Map* and most likely other mycobacteria. S-type strains contain an SNP in *bfaA* that prevents TBSA production and a knockout of *bfaA* in the C-type strains accomplishes the same phenotype. These results, combined with those from other studies examining *Map* lipids within macrophages (13), strongly suggest that TBSA is not essential for *in vitro* growth in media or cultured macrophages. S-type strains have also been isolated from goats and sheep (21), suggesting TBSA is not necessary in that environment either. Studies suggest that TBSA regulates membrane fluidity (34, 35), but mycobacteria appear to be able to compensate for lack of TBSA using other means to regulate membrane dynamics.

The differential production of TBSA in S-type and C-type strains is an example of a clear genotypic difference that results in a demonstrable change in membrane lipid composition. This further illustrates the differences in the cell wall lipid content of *Map* S-type and C-type strains above what has been noted previously by our group (6). We previously identified another substantial difference that exists in cell wall peptidolipids

A

```
Map C-type K-10           1201 TGGTCGTCGGTGCCCGCCGGTGCGACCGAGGGCGCCACCAACCGGCTGATCGAAGCCAAG 1260
Map C-type MAPK_JB16/15   1201 TGGTCGTCGGTGCCCGCCGGTGCGACCGAGGGCGCCACCAACCGGCTGATCGAAGCCAAG 1260
Map C-type MAP4           1201 TGGTCGTCGGTGCCCGCCGGTGCGACCGAGGGCGCCACCAACCGGCTGATCGAAGCCAAG 1260
Map C-type 10_4404        1201 TGGTCGTCGGTGCCCGCCGGTGCGACCGAGGGCGCCACCAACCGGCTGATCGAAGCCAAG 1260
  Map S-type Telford      1201 TG-TCGTCGGTGCCCGCCGGTGCGACCGAGGGCGCCACCAACCGGCTGATCGAAGCCAAG 1259
  Map S-type JIII-386     1201 TG-TCGTCGGTGCCCGCCGGTGCGACCGAGGGCGCCACCAACCGGCTGATCGAAGCCAAG 1259
  Map S-type S397         1201 TG-TCGTCGGTGCCCGCCGGTGCGACCGAGGGCGCCACCAACCGGCTGATCGAAGCCAAG 1259
  Map S-type S467         1201 TG-TCGTCGGTGCCCGCCGGTGCGACCGAGGGCGCCACCAACCGGCTGATCGAAGCCAAG 1259
  Map S-type LN20         1201 TG-TCGTCGGTGCCCGCCGGTGCGACCGAGGGCGCCACCAACCGGCTGATCGAAGCCAAG 1259
  Map S-type 11_1786      1201 TG-TCGTCGGTGCCCGCCGGTGCGACCGAGGGCGCCACCAACCGGCTGATCGAAGCCAAG 1259
  Map S-type 08_8281      1200 TG-TCGTCGGTGCCCGCCGGTGCGACCGAGGGCGCCACCAACCGGCTGATCGAAGCCAAG 1258
    Maa ATCC25291         1201 TGGTCGTCGGTGCCCGCCGGTGCGACCGAGGGCGCCACCAACCGGCTGATCGAAGCCAAG 1260
    Maa 05_4293           1201 TGGTCGTCGGTGCCCGCCGGTGCGACCGAGGGCGCCACCAACCGGCTGATCGAAGCCAAG 1260
    Maa 10_5581           1201 TGGTCGTCGGTGCCTGCCGGTGCGACCGAGGGCGCCACCAACCGGCTGATCGAAGCCAAG 1260
    Mah OCU464            1201 TGGTCGTCGGTGCCCGCCGGTGCGACCGAGGGCGCCACCAACCGGCTGATCGAAGCCAAG 1260
    Mah strain 104        1201 TGGTCGTCGGTGCCCGCCGGTGCGACCGAGGGCGCCACCAACCGGCTGATCGAAGCCAAG 1260
    Mas ATCC49884         1201 TGGTCGTCGGTGCCCGCCGGTGCGACCGAGGGCGCCACCAACCGGCTGATCGAAGCCAAG 1260
                               ** ********** ********************************************
```
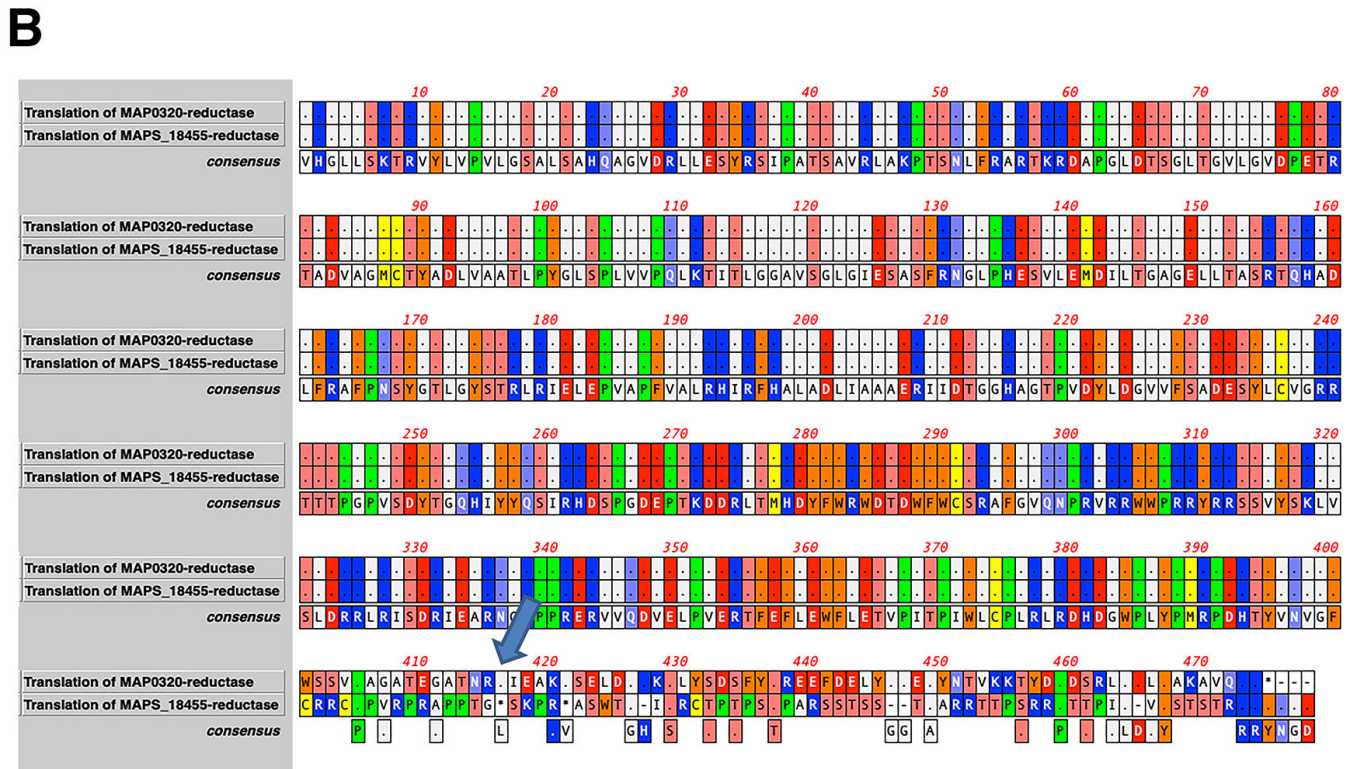
B

FIG 6 Sequence alignment of *bfaA* in *M. avium* subspecies strains. (A) Shown are the *bfaA* sequences from coordinates 1201–1260 in four C-type *Map* (top), seven S-type *Map* (middle), and six non-*Map M. avium* subspecies strains (bottom). The SNP is shown boxed in red, represented by a dash for the missing guanine nucleotide. The TGA, also boxed in red, shows the location of the stop codon that is in frame only in the S-type strains. The asterisks across the bottom represents 100% conservation of the nucleotide at that position. (B) Amino acid alignment of BfaA in *Map* K-10 (top) and *Map* S397 (middle) with the consensus sequence is at the bottom. The blue arrow denotes the position of the premature stop codon (416) in the S-type strain. The SNP shifts the reading frame at amino acid 401 [TGG (W) to TGT (C)].

between these strain types, which has similarly been traced to a defined genetic difference. The C-type strains contain an antigenic lipopentapeptide molecule, while the S-type strains contain a lipotripeptide which can be traced to a multi-kilobase deletion of two modules with a large non-ribosomal peptide synthase gene (6, 10, 50). In the current study, TBSA production was not only controlled by a genetic lesion in S-type
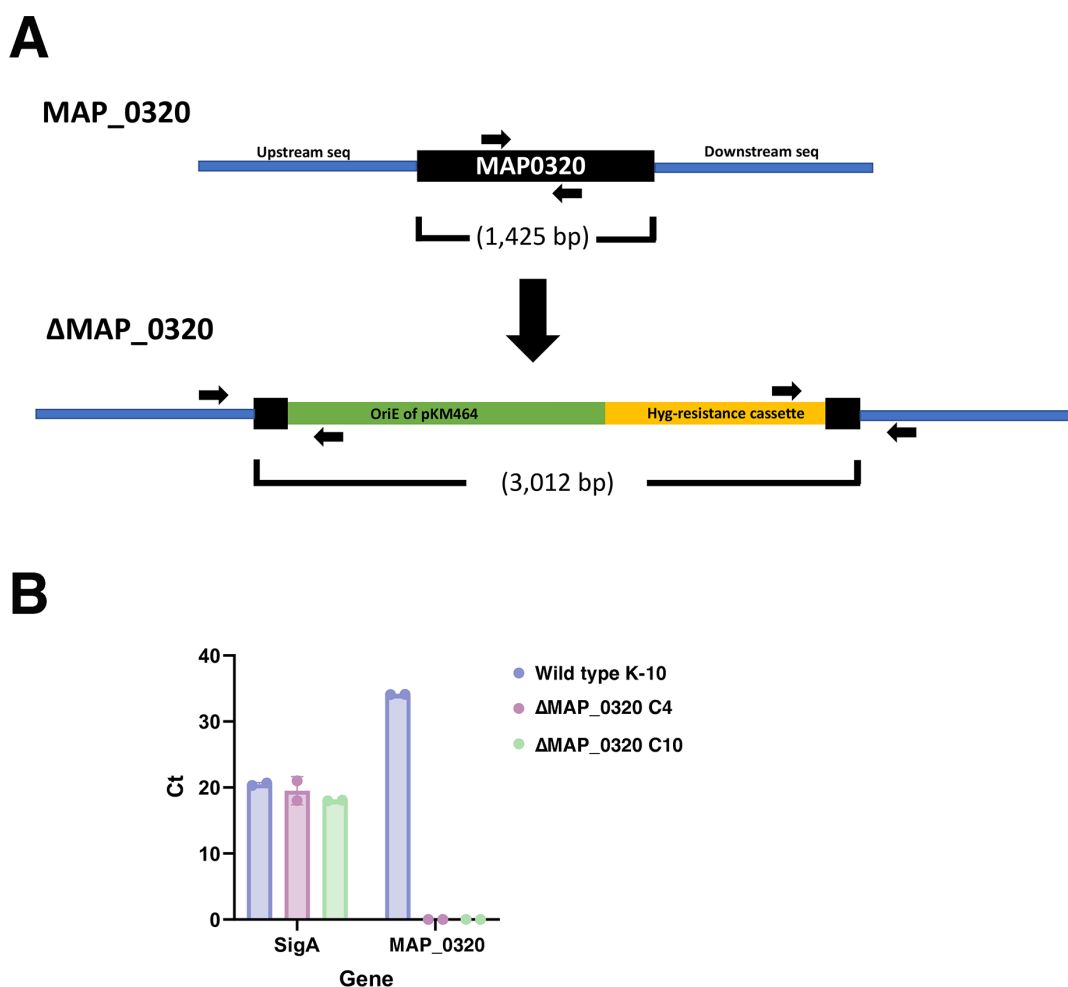
FIG 7 Construction and confirmation of the ΔMAP_0320 knockout. (A) Schematic showing the MAP_320 gene locus in the wild-type and knockout strains. Replacement of the *bfaA* gene was accomplished with an integrating plasmid. The origin of replication for the pKM464 plasmid is shown for the mutant in green, while the hygromycin resistance cassette is shown in yellow. The gene size, as well as the size of the integrated pKM464 plasmid and remanent *bfaA* sequence (black), is indicated in base pairs. Black arrows show primer positions. (B) RT-PCR analysis of the ΔMAP_0320 knockouts and the wild-type K-10 strain. Although MAP_0320 transcripts were detected in the wild type, no transcripts were detected in the knockout mutants, indicating a loss of expression for that gene and confirming the ΔMAP_0320 knockout. The *sigA* gene was used as a control to demonstrate equivalent RNAs and ability to amplify transcripts from each strain. Ct, cycle threshold.

strains but also could be chemically controlled using pivalic acid. Media supplemented with increasing concentrations of pivalic acid show a dose-dependent inhibition of TBSA production with all mycobacteria tested, but the tolerance of pivalic acid varies among species and even subspecies. These combined factors highlight the need for caution if TBSA is used as a diagnostic marker for *Map* as it has been used extensively for *M. tuberculosis* (39, 40).

M. avium strains cultured with increasing concentrations of pivalic acid showed remarkable effects on cellular fatty acid production, especially myristic and oleic acids as well as TBSA. It is interesting to note that the S-type strains are more sensitive to pivalic acid even though they inherently lack the ability to produce TBSA. This may suggest that lack of TBSA production is a secondary effect of pivalic acid presence, and the specific mode of action that inhibits growth remains unknown. Mechanistically, it is also unclear how pivalic acid prevents TBSA production. Pivalic acid is a short-chain organic acid that gets incorporated into fatty acids directly in some bacteria but not in others. This primer unit for fatty acid biosynthesis is used in *Rhodococcus*, *Streptomyces* (29), and *Bacillus cereus* but not in other bacteria (30). Much less is known about pivalic
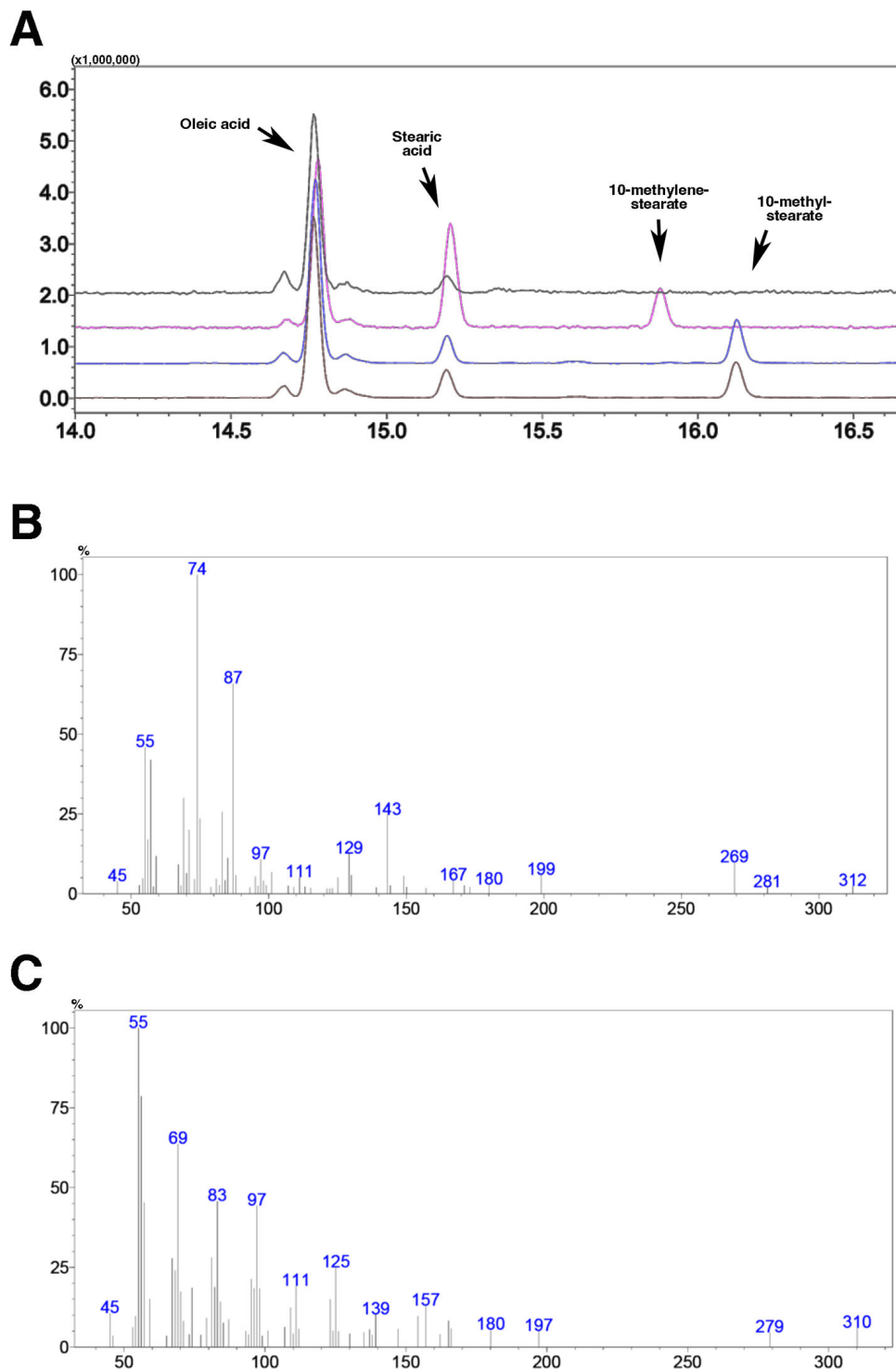
FIG 8 GC/MS and EI on FAMEs of the ΔMAP_0320 knockout. The GC/MS spectra in panel A shows the Middlebrook media alone (top trace), K-10 transformed with the pKM444 plasmid (second line, magenta), the C4 knockout (third blue trace), and the C10 knockout (bottom line). Both knockouts show the 10-methylene stearate peak at 16.1 min, while the K-10 strain shows the TBSA peak at 15.9 min. Relevant fatty acids are indicated on the spectra. EI was used in GC/MS to confirm the 10-methyl-stearate obtained from K-10 transformed with pKM444 (B) and the 10-methylene-stearate from the C4 knockout (C). The spectra in panel B was taken at 15.86 min, and the spectra in panel C was taken at 16.12 min. EI, electron ionization.

acid incorporation into mycobacterial fatty acids. Perhaps this inhibition is caused by something in the reductase step since there is an increase in the stearic acid concomitant with the decrease in TBSA.

Although *Mah* has a higher MIC (32 mg/mL) than *Map*, pivalic acid inhibits growth by 20% for both subspecies at the 0.5-mg/mL concentration. *M. smegmatis* remains unaffected at this concentration. In fact, low concentrations of pivalic acid were stimulatory for *M. smegmatis*. This observation was surprising, given that *M. smegmatis* generally shows more sensitivity to compounds than *Map*. For example, a cocktail of antibiotics is used for primary isolation of *Map* due to its natural resistance (51, 52), and directly comparing one antibiotic, ceftazidime, the MIC is 1 mg/mL in *Map* K10 (unpublished results), and for *M. smegmatis*, it is about 0.256 mg/mL (53). Perhaps the ratio of oleic acid and stearic acid, which hit an inversion point with increasing pivalic acid concentrations for *Map* (Fig. 3A and B), somehow changes the growth from stimulatory to inhibitory. This is a classical hormetic response where a compound is stimulatory at low doses but becomes inhibitory at higher doses. This type of response was recently noted with 13 antimicrobial peptides that stimulated *Map* growth at low concentrations (54). Regardless, the sensitivity of *Map* suggests there may be a role for pivalic acid as a therapeutic for Johne's disease or at least for controlling production of this industrially important fatty acid.

In contrast, our group previously demonstrated that *B. cereus* grew well on pivalic acid up to a concentration of 2.0 mg/mL in liquid culture (30). Concentrations above this level were not tested in that study, but results from this study suggest an interesting hypothesis of whether high-dose pivalic acid could ultimately affect *Bacillus* growth. Furthermore, *B. cereus* incorporated pivalic acid in its cellular lipids, whereas *Bacillus subtilis* did not (30). Therefore, although *Map* is generally quite resistant to antibiotics, such as the β-lactams, it does appear to be sensitive to pivalic acid, which is not considered an antibacterial agent. While the blocking of TBSA production with this short-chain fatty acid has not been reported in the literature, it is known that other fatty acid derivatives, mostly long-chain fatty acids with a C18 carbon backbone, inhibit *Map* growth (55). However, the question of why this short-carbon chain compound inhibits mycobacteria remains to be answered. One possibility is that co-enzyme A pools are being used up as pivalic acid-CoA, since acetyl-CoA has a high-energy bond that is particularly reactive due to the exergonic thioester bond. If the thioester-linked acetate group is replaced by the pivalic acid group, this would theoretically be more stable. Then, higher pivalic acid concentrations could use up all the available CoA needed for viability. However, the bond energy calculations showed no significant difference between acetyl-CoA and pivalate-CoA.

In *Corynebacterium* species, the 10-methylene stearate intermediate is consistently detected by GC/MS; however, one rare β-lactam-susceptible strain did not contain the intermediate but had more abundant TBSA (38). The mechanism behind this observation was never revealed; however, this genus appears to differentially contain the *bfa* gene operon as *Corynebacterium renale* does not contain the genes in its genome, while *Corynebacterium glyciniphilum* does (36). Likewise, taxonomically, only some strains of *Corynebacterium* produce TBSA, and they have been grouped under the species name *Corynebacterium tuberculostearicum* (56). It would be interesting to conduct sequence alignments of these corynebacterial species to correlate presence/absence of *bfa* genes with TBSA production. In *Mycobacterium*, the intermediate is generally not detected, with the notable exception of the S-type strains of *Map* where it is readily detected.

Alonso-Hearn and co-workers previously examined FAMEs in *Map* and also observed a lack of TBSA production in a single S-type strain isolated from sheep in Portugal (13). They further showed that TBSA is not produced in that strain regardless of their environment as they examined *Map* in macrophages and culture media (13). However, they did not determine the subtype of the strain (subtype I or subtype III). This study confirms and expands those findings as we now know that the lack of TBSA production is universal among subtype I and III strains and that the fatty acid differences are attributed

to an SNP in these strains rather than influenced by the environment. Therefore, TBSA could be used as a chemical marker to distinguish the C-type from S-type strains of *Map*.

The S-type strains are known to grow at slower rates, and they survive in macrophages at lower CFUs than the C-type strains (57–61). The two S-type strains used in this study grow slower than the C-type strains, and they both lack TBSA in all tested conditions. It would be tempting to propose that the slow growth of the sheep strains is due to the lack of TBSA production, but since we have the C4 and C10 knockouts in the C-type strain, which also do not produce TBSA but do grow at a similar rate to C-type strains, this argument is nullified. While we could not directly test the ability of subtype I strains to produce TBSA, we hypothesize that they will not due to the presence of an identical SNP observed in the subtype III strains. Currently, no type I strains have been isolated in the United States; however, they are present in Australia and parts of Europe. The host that *Map* is isolated from is not as important as the strain type as two C-type strains isolated from different sheep breeds produced TBSA in the absence of pivalic acid and did not possess the SNP in *bfaA* as other sheep isolates did.

The *bfaA* knockouts examined in this study prevented TBSA production in C-type *Map*. Our work demonstrates that the FAD-binding domain is the oxidoreductase necessary to mediate the second step in the biosynthesis of TBSA, where 10-methylene stearate is reduced. Without this enzyme, the intermediate is detectable by GC, but a fully functional BfaA shows only TBSA and not the intermediate (Fig. 8). We also demonstrate that *Map bfaA* and *bfaB* are co-transcribed in a two-gene operon. With any gene knockout, its polar effect must be considered especially when that gene is present within an operon. However, the *Map* knockout was completely contained within *bfaA*, and GC/MS analysis showed that the intermediate is still produced (Fig. 8), confirming the knockout did not have a downstream effect on *bfaB*. Another study examined a knockout of *bfaB* in *M. smegmatis*, which they designated *cfa* (35). They showed the *cfa* knockout altered the phosphatidylinositol mannosides in *M. smegmatis* and affected membrane fluidity in an unknown way. Furthermore, they demonstrated that BfaB may have modifying effects on 62 polar lipids of *M. smegmatis* (35). When TBSA was not produced by the *M. smegmatis cfa* knockout, oleic acid was incorporated into phospholipids instead.

Our data demonstrate that the mycobacteria convert stearic acid, which is depleted in growing cultures, to oleic acid, which increased in growing cultures. Oleic acid is subsequently converted to TBSA. However, when mycobacterial growth is inhibited by pivalic acid, there is a decrease in both oleic acid and TBSA. Oleic acid is an important component of mycobacterial membrane phospholipids, where it likely plays a role in membrane physiology (62). Oleic acid is a component in the OADC media supplement routinely used to culture *Map*. Conversely ADC, which is missing only the oleic acid component, is used for cultivation of fast-growing mycobacteria, such as *M. smegmatis*. A recent study suggested that ADC supplement enhanced growth of *Map* more so than OADC under certain media formulations (63), and although we did not observe enhanced growth, the bovine strains tested in this study grew to similar yields in ADC-supplemented versus OADC-supplemented media. However, the presence of exogenous oleic acid, a starting substrate for TBSA biosynthesis, had no effect on TBSA production. Testing for *M. tuberculosis* growth in ADC versus OADC supplements has also been done previously to demonstrate that oleic acid can reverse the bactericidal effect of thiocarlide, a thiourea compound (64). Thiocarlide is a strong inhibitor of *M. tuberculosis*, and its effect decreases oleic acid and concomitantly TBSA, as well as mycolic acids (64, 65).

Fatty acids in biological membranes are commonly analyzed by gas chromatography (GC), but they must first be esterified before GC analysis. FAMEs analyzed in this study show that bovine strains of *Map* exposed to pivalic acid do not produce TBSA. The changes in fatty acid composition of *Map* can affect the amount of mannose on the cell surface and/or might change the nature or location of mannose in the cell envelope (13, 35). Fatty acid methyl esters can yield limited structural information by GC/MS as it

does not show carbon-carbon bond cleavage, which allows localization of double bonds and other side-chain moieties. In this regard, some have suggested it is better to do picolinyl esters, especially for branched-chain fatty acids (29). These esters can be difficult to prepare, however. Pyrrolidides for MS can resolve the position of double bonds in monounsaturated fatty acids (66). We used this method on the deuterated TBSA that resulted in reduction of the 10-methylene stearate with sodium borodeuteride. This approach gave excellent resolution.

Given that TBSA is a prominent fatty acid in the cell wall of mycobacteria (31), it was of interest to determine if the lack of TBSA production resulted in any observable morphological changes in *Map*. Transmission electron microscopy results show that *Map* C-type strains look the same as the S-type strains, and the mutants looked similar to the parent strain. Therefore, except for lack of TBSA production, this mutation appears to be silent with respect to growth and morphology. It is still unknown how the strains that do not produce TBSA are affected. The S-type strains can still infect sheep, and the C-type knockout appears to have the same growth rate in Middlebrook media as other C-type strains. Obviously, *bfaA* is not an essential gene in *Map* and does not appear to affect cell wall morphology or growth using the conditions in this study.

ACKNOWLEDGMENTS

AUTHOR AFFILIATIONS

[1]National Animal Disease Center, USDA Agricultural Research Service, Ames, Iowa, USA
[2]Department of Microbiology and Immunology, McGill University, Montreal, Quebec, Canada
[3]ARS Participation Program, Oak Ridge Institute for Science and Education (ORISE), Oak Ridge, Tennessee, USA
[4]INRAE, ISP, Université de Tours, Nouzilly, France
[5]National Center for Agricultural Utilization Research, USDA Agricultural Research Service, Peoria, Illinois, USA

AUTHOR ORCIDs

John P. Bannantine http://orcid.org/0000-0002-5692-7898
Shannon C. Duffy http://orcid.org/0000-0003-2296-9907
Marcel A. Behr http://orcid.org/0000-0003-0402-4467
Franck Biet http://orcid.org/0000-0001-8425-6158

FUNDING

AUTHOR CONTRIBUTIONS

John P. Bannantine, Conceptualization, Data curation, Formal analysis, Funding acquisition, Investigation, Methodology, Project administration, Resources, Supervision, Validation, Visualization, Writing – original draft | Shannon C. Duffy, Investigation, Methodology, Writing – review and editing | María A. Colombatti Olivieri, Data curation, Formal analysis, Investigation, Methodology | Marcel A. Behr, Investigation, Methodology,

Resources, Writing – review and editing | Franck Biet, Methodology, Resources, Writing – review and editing | Neil P. J. Price, Data curation, Formal analysis, Investigation, Methodology, Resources, Writing – review and editing

DATA AVAILABILITY

The shotgun genome sequence for *Mycobacterium smegmatis* used in this study was deposited under the National Center for Biotechnology Information accession number NZ_JALHLC010000018. RNA-Seq data were obtained through the BioProject ID PRJNA1074775.

ADDITIONAL FILES

The following material is available online.

Supplemental Material

Supplemental material (Spectrum00508-24-s0001.pdf). Fig. S1 to S10; Tables S1 to S8.

REFERENCES

1. Shin MK, Shin SJ. 2021. Genetic involvement of *Mycobacterium avium* complex in the regulation and manipulation of innate immune functions of host cells. Int J Mol Sci 22:3011. https://doi.org/10.3390/ijms22063011
2. Stevenson K. 2015. Genetic diversity of *Mycobacterium avium* subspecies *paratuberculosis* and the influence of strain type on infection and pathogenesis: a review. Vet Res 46:64. https://doi.org/10.1186/s13567-015-0203-2
3. Mizzi R, Timms VJ, Price-Carter ML, Gautam M, Whittington R, Heuer C, Biggs PJ, Plain KM. 2021. Comparative genomics of *Mycobacterium avium* subspecies *paratuberculosis* sheep strains. Front Vet Sci 8:637637. https://doi.org/10.3389/fvets.2021.637637
4. Lim J, Park HT, Ko S, Park HE, Lee G, Kim S, Shin MK, Yoo HS, Kim D. 2021. Genomic diversity of *Mycobacterium avium* subsp. *paratuberculosis*: pangenomic approach for highlighting unique genomic features with newly constructed complete genomes. Vet Res 52:46. https://doi.org/10.1186/s13567-021-00905-1
5. Castellanos E, Aranaz A, Romero B, de Juan L, Alvarez J, Bezos J, Rodríguez S, Stevenson K, Mateos A, Domínguez L. 2007. Polymorphisms in *gyrA* and *gyrB* genes among *Mycobacterium avium* subsp. *paratuberculosis* type I, II, and III isolates. J Clin Microbiol 45:3439–3442. https://doi.org/10.1128/JCM.01411-07
6. Bannantine JP, Etienne G, Laval F, Stabel JR, Lemassu A, Daffé M, Bayles DO, Ganneau C, Bonhomme F, Branger M, Cochard T, Bay S, Biet F. 2017. Cell wall peptidolipids of *Mycobacterium avium*: from genetic prediction to exact structure of a nonribosomal peptide. Mol Microbiol 105:525–539. https://doi.org/10.1111/mmi.13717
7. de Juan L, Mateos A, Domínguez L, Sharp JM, Stevenson K. 2005. Genetic diversity of *Mycobacterium avium* subspecies *paratuberculosis* isolates from goats detected by pulsed-field gel electrophoresis. Vet Microbiol 106:249–257. https://doi.org/10.1016/j.vetmic.2004.12.013
8. Biet F, Sevilla IA, Cochard T, Lefrançois LH, Garrido JM, Heron I, Juste RA, McLuckie J, Thibault VC, Supply P, Collins DM, Behr MA, Stevenson K. 2012. Inter- and intra-subtype genotypic differences that differentiate *Mycobacterium avium* subspecies *paratuberculosis* strains. BMC Microbiol 12:264. https://doi.org/10.1186/1471-2180-12-264
9. Sparks IL, Derbyshire KM, Jacobs WR, Morita YS. 2023. *Mycobacterium smegmatis*: the vanguard of mycobacterial research. J Bacteriol 205:e0033722. https://doi.org/10.1128/jb.00337-22
10. Biet F, Bay S, Thibault VC, Euphrasie D, Grayon M, Ganneau C, Lanotte P, Daffé M, Gokhale R, Etienne G, Reyrat J-M. 2008. Lipopentapeptide induces a strong host humoral response and distinguishes *Mycobacterium avium* subsp. *paratuberculosis* from *M. avium* subsp. *avium*. Vaccine 26:257–268. https://doi.org/10.1016/j.vaccine.2007.10.059
11. Hosseiniporgham S, Biet F, Ganneau C, Bannantine JP, Bay S, Sechi LA. 2021. A comparative study on the efficiency of two *Mycobacterium avium* subsp. *paratuberculosis* (MAP)-derived lipopeptides of L3P and L5P as capture antigens in an in-house milk ELISA test. Vaccines (Basel) 9:997. https://doi.org/10.3390/vaccines9090997
12. Thoen CO, Karlson AG, Ellefson RD. 1971. Comparison by gas-liquid chromatography of the fatty acids acids of *Mycobacterium avium* and some other nonphotochromogenic mycobacteria. Appl Microbiol 22:560–563. https://doi.org/10.1128/am.22.4.560-563.1971
13. Alonso-Hearn M, Abendaño N, Ruvira MA, Aznar R, Landin M, Juste RA. 2017. *Mycobacterium avium* subsp. *paratuberculosis* (*Map*) fatty acids profile is strain-dependent and changes upon host macrophages infection. Front Cell Infect Microbiol 7:89. https://doi.org/10.3389/fcimb.2017.00089
14. Gumber S, Taylor DL, Marsh IB, Whittington RJ. 2009. Growth pattern and partial proteome of *Mycobacterium avium* subsp. *paratuberculosis* during the stress response to hypoxia and nutrient starvation. Vet Microbiol 133:344–357. https://doi.org/10.1016/j.vetmic.2008.07.021
15. Sohal JS, Arsenault J, Leboeuf A, Hélie P, Buczinski S, Robinson Y, Labrecque O, Lachapelle V, Fecteau G, L'Homme Y. 2019. Molecular characterization of *Mycobacterium avium* subspecies *paratuberculosis* C-type and S-type isolated from sheep and goats by using a combination of MIRU-VNTR loci. Can J Vet Res 83:160–167.
16. Whittington RJ, Marsh IB, Saunders V, Grant IR, Juste R, Sevilla IA, Manning EJB, Whitlock RH. 2011. Culture phenotypes of genomically and geographically diverse *Mycobacterium avium* subsp. *paratuberculosis* isolates from different hosts. J Clin Microbiol 49:1822–1830. https://doi.org/10.1128/JCM.00210-11
17. Rasper-Hössinger M, Biggel M, Stephan R, Seehusen F, Scherrer S. 2023. Strain diversity in *Mycobacterium avium* subsp. *paratuberculosis*-positive bovine fecal samples collected in Switzerland. Front Vet Sci 10:1154516. https://doi.org/10.3389/fvets.2023.1154516
18. Szteyn J, Wiszniewska-Łaszczych A, Wojtacka J, Wysok B, Liedke K. 2020. Short communication: occurrence and differentiation of *Mycobacterium avium* ssp. *paratuberculosis* (MAP) strains from milk of cows from herd with low prevalence of MAP. J Dairy Sci 103:8526–8529. https://doi.org/10.3168/jds.2019-16816
19. Conde C, Thézé J, Cochard T, Rossignol M-N, Fourichon C, Delafosse A, Joly A, Guatteo R, Schibler L, Bannantine JP, Biet F. 2022. Genetic features of *Mycobacterium avium* subsp. *paratuberculosis* strains circulating in the west of France deciphered by whole-genome sequencing. Microbiol Spectr 10:e0339222. https://doi.org/10.1128/spectrum.03392-22
20. Möbius P, Luyven G, Hotzel H, Köhler H. 2008. High genetic diversity among *Mycobacterium avium* subsp. *paratuberculosis* strains from German cattle herds shown by combination of IS900 restriction fragment length polymorphism analysis and mycobacterial interspersed repetitive unit-variable-number tandem-repeat typing. J Clin Microbiol 46:972–981. https://doi.org/10.1128/JCM.01801-07

21. Bauman CA, Jones-Bitton A, Ahlstrom C, Mutharia L, De Buck J, Jansen J, Kelton D, Menzies P. 2017. Identification of *Mycobacterium avium* subspecies *paratuberculosis* strains isolated from dairy goats and dairy sheep in Ontario, Canada. Can J Vet Res 81:304–307.

22. Motiwala AS, Amonsin A, Strother M, Manning EJB, Kapur V, Sreevatsan S. 2004. Molecular epidemiology of *Mycobacterium avium* subsp. *paratuberculosis* isolates recovered from wild animal species. J Clin Microbiol 42:1703–1712. https://doi.org/10.1128/JCM.42.4.1703-1712.2004

23. Janagama HK, Senthilkumar TMA, Bannantine JP, Rodriguez GM, Smith I, Paustian ML, McGarvey JA, Sreevatsan S. 2009. Identification and functional characterization of the iron-dependent regulator (IdeR) of *Mycobacterium avium* subsp. *paratuberculosis*. Microbiology (Reading) 155:3683–3690. https://doi.org/10.1099/mic.0.031948-0

24. Lefrancois LH, Bodier CC, Cochard T, Canepa S, Raze D, Lanotte P, Sevilla IA, Stevenson K, Behr MA, Locht C, Biet F. 2013. Novel feature of *Mycobacterium avium* subsp. *paratuberculosis*, highlighted by characterization of the heparin-binding hemagglutinin adhesin. J Bacteriol 195:4844–4853. https://doi.org/10.1128/JB.00671-13

25. Fernández M, Benavides J, Sevilla IA, Fuertes M, Castaño P, Delgado L, García Marín JF, Garrido JM, Ferreras MC, Pérez V. 2014. Experimental infection of lambs with C and S-type strains of *Mycobacterium avium* subspecies *paratuberculosis*: immunological and pathological findings. Vet Res 45:5. https://doi.org/10.1186/1297-9716-45-5

26. Marsh IB, Bannantine JP, Paustian ML, Tizard ML, Kapur V, Whittington RJ. 2006. Genomic comparison of *Mycobacterium avium* subsp. *paratuberculosis* sheep and cattle strains by microarray hybridization. J Bacteriol 188:2290–2293. https://doi.org/10.1128/JB.188.6.2290-2293.2006

27. Price NPJ, Jackson MA, Hartman TM, Branden G, Ek M, Koch AA, Kennedy PD. 2021. Branched chain lipid metabolism as a determinant of the *N*-acyl variation of *Streptomyces* natural products. ACS Chem Biol 16:116–124. https://doi.org/10.1021/acschembio.0c00799

28. Rezanka T, Kolouchová I, Cejková A, Sigler K. 2012. Biosynthesis and metabolic pathways of pivalic acid. Appl Microbiol Biotechnol 95:1371–1376. https://doi.org/10.1007/s00253-012-4267-x

29. Rezanka T, Siristova L, Schreiberová O, Rezanka M, Masák J, Melzoch K, Sigler K. 2011. Pivalic acid acts as a starter unit in a fatty acid and antibiotic biosynthetic pathway in *Alicyclobacillus*, *Rhodococcus* and *Streptomyces*. Environ Microbiol 13:1577–1589. https://doi.org/10.1111/j.1462-2920.2011.02465.x

30. Price NPJ, Jackson MA, Hartman TM, Bannantine JP, Naumann TA, Vermillion KE, Koch AA, Kennedy PD. 2023. Precursor-directed biosynthesis and biological testing of *omega*-alicyclic- and *neo*-branched tunicamycin *N*-acyl variants. ACS Chem Biol 18:2267–2280. https://doi.org/10.1021/acschembio.3c00324

31. Daffé M, Marrakchi H. 2019. Unraveling the structure of the mycobacterial envelope. Microbiol Spectr 7. https://doi.org/10.1128/microbiolspec.GPP3-0027-2018

32. Brülle JK, Tschumi A, Sander P. 2013. Lipoproteins of slow-growing mycobacteria carry three fatty acids and are *N*-acylated by apolipoprotein *N*-acyltransferase BCG_2070c. BMC Microbiol 13:223. https://doi.org/10.1186/1471-2180-13-223

33. Bai W, Geng W, Wang S, Zhang F. 2019. Biosynthesis, regulation, and engineering of microbially produced branched biofuels. Biotechnol Biofuels 12:84. https://doi.org/10.1186/s13068-019-1424-9

34. Suutari M, Laakso S. 1993. Effect of growth temperature on the fatty acid composition of *Mycobacterium phlei*. Arch Microbiol 159:119–123. https://doi.org/10.1007/BF00250270

35. Prithviraj M, Kado T, Mayfield JA, Young DC, Huang AD, Motooka D, Nakamura S, Siegrist MS, Moody DB, Morita YS. 2023. Tuberculostearic acid controls mycobacterial membrane compartmentalization. mBio 14:e0339622. https://doi.org/10.1128/mbio.03396-22

36. Blitzblau HG, Consiglio AL, Teixeira P, Crabtree DV, Chen S, Konzock O, Chifamba G, Su A, Kamineni A, MacEwen K, Hamilton M, Tsakraklides V, Nielsen J, Siewers V, Shaw AJ. 2021. Production of 10-methyl branched fatty acids in yeast. Biotechnol Biofuels 14:12. https://doi.org/10.1186/s13068-020-01863-0

37. Machida S, Bakku RK, Suzuki I. 2017. Expression of genes for a flavin adenine dinucleotide-binding oxidoreductase and a methyltransferase from *Mycobacterium chlorophenolicum* is necessary for biosynthesis of 10-methyl stearic acid from oleic acid in *Escherichia coli* Front Microbiol 8:2061. https://doi.org/10.3389/fmicb.2017.02061

38. Couderc F, De Briel D, Demont N, Gilard V, Promé JC. 1991. Mass spectrometry as a tool for identifying group D2 corynebacteria by their fatty acid profiles. J Gen Microbiol 137:1903–1909. https://doi.org/10.1099/00221287-137-8-1903

39. Brandenburg J, Heyckendorf J, Marwitz F, Zehethofer N, Linnemann L, Gisch N, Karaköse H, Reimann M, Kranzer K, Kalsdorf B, Sanchez-Carballo P, Weinkauf M, Scholz V, Malm S, Homolka S, Gaede KI, Herzmann C, Schaible UE, Hölscher C, Reiling N, Schwudke D. 2022. Tuberculostearic acid-containing phosphatidylinositols as markers of bacterial burden in tuberculosis. ACS Infect Dis 8:1303–1315. https://doi.org/10.1021/acsinfecdis.2c00075

40. Cai G, Pauli GF, Wang Y, Jaki BU, Franzblau SG. 2013. Rapid determination of growth inhibition of *Mycobacterium tuberculosis* by GC-MS/MS quantitation of tuberculostearic acid. Tuberculosis (Edinb) 93:322–329. https://doi.org/10.1016/j.tube.2012.12.004

41. Etienne G, Laval F, Villeneuve C, Dinadayala P, Abouwarda A, Zerbib D, Galamba A, Daffé M. 2005. The cell envelope structure and properties of *Mycobacterium smegmatis* mc²155: is there a clue for the unique transformability of the strain? Microbiology (Reading) 151:2075–2086. https://doi.org/10.1099/mic.0.27869-0

42. Akamatsu Y, Law JH. 1968. Enzymatic synthesis of 10-methylene stearic acid and tuberculostearic acid. Biochem Biophys Res Commun 33:172–176. https://doi.org/10.1016/0006-291x(68)90274-x

43. Vogetseder W, Schratzberger E, Allerberger F, Dierich MP, Schmutzhard E. 1995. Evaluation of polymerase chain reaction (PCR) and determination of tuberculostearic acid for detection of *Mycobacterium leprae* in urine and cereprospinal fluid. Mitteilungen der Österreichischen Gesellschaft für Tropenmedizin und Parasitologie 17:195–200.

44. Teng LJ, Liaw SJ, Hsueh PR, Fan JH, Luh KT, Ha SW. 1997. Constitutive fatty acid and enzyme profiles of *Mycobacterium* species. J Formos Med Assoc 96:336–345.

45. Khoo KH, Dell A, Morris HR, Brennan PJ, Chatterjee D. 1995. Structural definition of acylated phosphatidylinositol mannosides from *Mycobacterium tuberculosis*: definition of a common anchor for lipomannan and lipoarabinomannan. Glycobiology 5:117–127. https://doi.org/10.1093/glycob/5.1.117

46. Bannantine JP, Huntley JFJ, Miltner E, Stabel JR, Bermudez LE. 2003. The *Mycobacterium avium* subsp. *paratuberculosis* 35 kDa protein plays a role in invasion of bovine epithelial cells. Microbiology 149:2061–2069. https://doi.org/10.1099/mic.0.26323-0

47. Murphy KC, Nelson SJ, Nambi S, Papavinasasundaram K, Baer CE, Sassetti CM. 2018. ORBIT: a new paradigm for genetic engineering of mycobacterial chromosomes. mBio 9:e01467-18. https://doi.org/10.1128/mBio.01467-18

48. Danecek P, Auton A, Abecasis G, Albers CA, Banks E, DePristo MA, Handsaker RE, Lunter G, Marth GT, Sherry ST, McVean G, Durbin R, 1000 Genomes Project Analysis Group. 2011. The variant call format and VCFtools. Bioinformatics 27:2156–2158. https://doi.org/10.1093/bioinformatics/btr330

49. Bisel P, Al-Momani L, Müller M. 2008. The tert-butyl group in chemistry and biology. Org Biomol Chem 6:2655–2665. https://doi.org/10.1039/b800083b

50. Eckstein TM, Chandrasekaran S, Mahapatra S, McNeil MR, Chatterjee D, Rithner CD, Ryan PW, Belisle JT, Inamine JM. 2006. A major cell wall lipopeptide of *Mycobacterium avium* subspecies *paratuberculosis*. J Biol Chem 281:5209–5215. https://doi.org/10.1074/jbc.M512465200

51. Florou M, Leontides L, Kostoulas P, Billinis C, Sofia M. 2009. Strain-specific sensitivity estimates of *Mycobacterium avium* subsp. *paratuberculosis* culture in Greek sheep and goats. Zoonoses Public Health 56:49–52. https://doi.org/10.1111/j.1863-2378.2008.01179.x

52. Whittington RJ. 2009. Factors affecting isolation and identification of *Mycobacterium avium* subsp. *paratuberculosis* from fecal and tissue samples in a liquid culture system. J Clin Microbiol 47:614–622. https://doi.org/10.1128/JCM.01986-08

53. Cotta KB, Ghosh S, Mehra S. 2022. Potentiating the anti-tuberculosis efficacy of peptide nucleic acids through combinations with permeabilizing drugs. Microbiol Spectr 10:e0126221. https://doi.org/10.1128/spectrum.01262-21

54. Hilpert K, Munshi T, López-Pérez PM, Sequeira-Garcia J, Hofmann S, Bull TJ. 2023. Discovery of antimicrobial peptides that can accelerate culture diagnostics of slow-growing mycobacteria including *Mycobacterium tuberculosis*. Microorganisms 11:2225. https://doi.org/10.3390/microorganisms11092225

55. Zinniel DK, Sittiwong W, Marshall DD, Rathnaiah G, Sakallioglu IT, Powers R, Dussault PH, Barletta RG. 2019. Novel amphiphilic cyclobutene and cyclobutane *cis*-C_{18} fatty acid derivatives inhibit *Mycobacterium avium* subsp. *paratuberculosis* growth. Vet Sci 6:46. https://doi.org/10.3390/vetsci6020046

56. Feurer C, Clermont D, Bimet F, Candréa A, Jackson M, Glaser P, Bizet C, Dauga C. 2004. Taxonomic characterization of nine strains isolated from clinical and environmental specimens, and proposal of *Corynebacterium tuberculostearicum* sp. nov. Int J Syst Evol Microbiol 54:1055–1061. https://doi.org/10.1099/ijs.0.02907-0

57. Sevilla I, Garrido JM, Geijo M, Juste RA. 2007. Pulsed-field gel electrophoresis profile homogeneity of *Mycobacterium avium* subsp. *paratuberculosis* isolates from cattle and heterogeneity of those from sheep and goats. BMC Microbiol 7:18. https://doi.org/10.1186/1471-2180-7-18

58. Collins DM, Gabric DM, de Lisle GW. 1990. Identification of two groups of *Mycobacterium paratuberculosis* strains by restriction endonuclease analysis and DNA hybridization. J Clin Microbiol 28:1591–1596. https://doi.org/10.1128/jcm.28.7.1591-1596.1990

59. Elguezabal N, Bastida F, Sevilla IA, González N, Molina E, Garrido JM, Juste RA. 2011. Estimation of *Mycobacterium avium* subsp. *paratuberculosis* growth parameters: strain characterization and comparison of methods. Appl Environ Microbiol 77:8615–8624. https://doi.org/10.1128/AEM.05818-11

60. Abendaño N, Sevilla IA, Prieto JM, Garrido JM, Juste RA, Alonso-Hearn M. 2013. *Mycobacterium avium* subspecies *paratuberculosis* isolates from sheep and goats show reduced persistence in bovine macrophages than cattle, bison, deer and wild boar strains regardless of genotype. Vet Microbiol 163:325–334. https://doi.org/10.1016/j.vetmic.2012.12.042

61. Abendaño N, Tyukalova L, Barandika JF, Balseiro A, Sevilla IA, Garrido JM, Juste RA, Alonso-Hearn M. 2014. *Mycobacterium avium* subsp. *paratuberculosis* isolates induce *in vitro* granuloma formation and show successful survival phenotype, common anti-inflammatory and antiapoptotic responses within ovine macrophages regardless of genotype or host of origin. PLoS One 9:e104238. https://doi.org/10.1371/journal.pone.0104238

62. Los DA, Murata N. 1998. Structure and expression of fatty acid desaturases. Biochim Biophys Acta 1394:3–15. https://doi.org/10.1016/s0005-2760(98)00091-5

63. Dane H, Koidis A, Stewart LD, Grant IR. 2022. Optimization of the composition of a solid culture medium for *Mycobacterium avium* subsp. *paratuberculosis* using factorial design and response surface methodology. J Appl Microbiol 132:4252–4265. https://doi.org/10.1111/jam.15517

64. Phetsuksiri B, Jackson M, Scherman H, McNeil M, Besra GS, Baulard AR, Slayden RA, DeBarber AE, Barry CE III, Baird MS, Crick DC, Brennan PJ. 2003. Unique mechanism of action of the thiourea drug isoxyl on *Mycobacterium tuberculosis*. J Biol Chem 278:53123–53130. https://doi.org/10.1074/jbc.M311209200

65. Phetsuksiri B, Baulard AR, Cooper AM, Minnikin DE, Douglas JD, Besra GS, Brennan PJ. 1999. Antimycobacterial activities of isoxyl and new derivatives through the inhibition of mycolic acid synthesis. Antimicrob Agents Chemother 43:1042–1051. https://doi.org/10.1128/AAC.43.5.1042

66. Andersson BA, Holman RT. 1974. Pyrrolidides for mass spectrometric determination of the position of the double bond in monounsaturated fatty acids. Lipids 9:185–190. https://doi.org/10.1007/BF02532690